Journal of Computational Mathematics
Vol.xx, No.x, 2025, 1–25.

http://www.global-sci.org/jcm
doi:10.4208/jcm.2505-m2024-0212

A SECOND-ORDER IN TIME AND ENERGY-DISSIPATIVE SCHEME FOR TIME-FRACTIONAL NAVIER-STOKES EQUATIONS*

Ruimin Gao and Dongfang Li[1)]
School of Mathematics and Statistics, Huazhong University of Science and Technology, Wuhan 430074, China;
Hubei Key Laboratory of Engineering Modeling and Scientific Computing, Huazhong University of Science and Technology, Wuhan 430074, China
Emails: ruimingao@hust.edu.cn, dfli@hust.edu.cn
Hongyu Qin
School of Mathematics and Physics, Wuhan Institute of Technology, Wuhan 430205, China
Email: qinhy@wit.edu.cn

Abstract

This paper proposes an energy-dissipative scheme for solving two- and three-dimensional time-fractional Navier-Stokes equations. The numerical scheme is constructed, using nonuniform $L2-1\sigma$ approximation in the temporal direction and the Fourier spectral method in the spatial direction. It is shown that the numerical scheme can keep discrete energy stable and the numerical solutions are uniformly bounded without any restriction on step sizes. Error estimates of the fully-discrete scheme are presented. Moreover, a fast algorithm is applied to accelerate the computation. Numerical results in long time intervals are presented to confirm the effectiveness and high efficiency of the scheme.

Mathematics subject classification: 11T23, 33F05, 35R11, 65M12.
Key words: Nonuniform $L2-1\sigma$ scheme, Time-fractional Navier-Stokes equation, Energy dissipation, Error estimates, Adaptive time stepping.

1. Introduction

We present an effective numerical scheme for solving the following time-fractional Navier-Stokes equation (TFNSE) with periodic boundary conditions:

$$\partial_t^\alpha \mathbf{u} - \nu\Delta\mathbf{u} + (\mathbf{u}\cdot\nabla)\mathbf{u} + \nabla p = 0, \quad \mathbf{x}\in\Omega, \quad t\in(0,T], \tag{1.1}$$

$$\nabla\cdot\mathbf{u} = 0, \quad \mathbf{x}\in\Omega, \quad t\in(0,T], \tag{1.2}$$

$$\mathbf{u} = \mathbf{u}_0(\mathbf{x}), \quad \mathbf{x}\in\bar{\Omega}, \quad t=0, \tag{1.3}$$

where $\Omega\subset\mathbb{R}^d$ $(d=2,3)$ is a rectangular domain, $T>0$ is a fixed time, $\nu>0$ is the viscosity parameter, the vector-valued function $\mathbf{u}$ represents the velocity, and the scalar function p is the pressure. Here ∂_t^α denotes the Caputo fractional derivative of order α $(0<\alpha<1)$ with respect to t, i.e.

$$\partial_t^\alpha \mathbf{u} = \frac{1}{\Gamma(1-\alpha)}\int_0^t \frac{\partial\mathbf{u}}{\partial r}\frac{1}{(t-r)^\alpha}dr.$$

* Received September 26, 2024 / Revised version received March 6, 2025 / Accepted May 12, 2025 / Published online November 24, 2025 /
[1)] Corresponding author

TFNSE is an effective mathematical model with which to describe the behavior of intermittent turbulence, where the flow field experiences sporadic, intense turbulent bursts amidst quieter intervals [11,42]. The Eqs. (1.1)-(1.3) can also be obtained by the notion of fractional velocity [3, 7,9,21], or viewed as a kind of fractional governing equations of incompressible flow [5,8,20,49]. In the past decades, theoretical analysis of the TFNSE has been extensive. Here we refer the reader to [44] for the uniqueness and existence of global and local mild solutions, to [4] for the well-posedness of TFNSE in $\mathbb{R}^N$ in Lebesgue space as well as the decay rates and regularity of the mild solutions.

It is remarkable that the solution of TFNSE possesses some fundamental properties. First, the solution of TFNSE has a certain initial layer, which is described by $\|\partial_t \mathbf{u}\| \leq Ct^{\alpha-1}$ [24,28, 40]. As $t \to 0^+$, $\partial_t \mathbf{u}$ blows up. Second, taking the inner product of (1.1) with $\mathbf{u}$ and acting the operator $\mathcal{I}_t^\alpha$ on both side of the equation, we get

$$\frac{1}{2}\|\mathbf{u}(t)\|^2 + \nu \mathcal{I}_t^\alpha \|\nabla \mathbf{u}(t)\|^2 \leq \frac{1}{2}\|\mathbf{u}_0\|^2, \tag{1.4}$$

where $\|\cdot\|$ presents the L^2-norm and

$$\big(\mathcal{I}_t^\alpha v\big)(t) := \int_0^t \frac{(t-s)^{\alpha-1}}{\Gamma(\alpha)} v(s) ds.$$

Eq. (1.4) implies that the equation satisfies the following energy dissipation. Especially, when $\alpha \to 1$, (1.4) covers the energy dissipation of the usual classical Navier-Stokes equation, namely,

$$\|\mathbf{u}(t)\|^2 \leq \|\mathbf{u}_0\|^2.$$

A significant amount of attention has been dedicated to the development of effective methods for overcoming the difficulties associated with the initial layer. Typical schemes include the L1 scheme [26,30,40] and nonuniform L2-type schemes [22,32], the convolution quadrature-type methods with some initial correction terms [18,19,27,45], and some transformed schemes with the change of variable [36,38]. Besides, there are also some structure-preserving schemes for time-fractional problems, see [6,12,15,43,48]. For instance, Tang *et al.* [41] studied the continuous and discrete energy dissipation laws for time-fractional phase-field equations. They also proposed a class of finite difference schemes to confirm the theoretical predictions. For solving the time fractional Allen-Cahn equations (TFACE), Liao *et al.* [33] established a nonuniform time-stepping $L2-1\sigma$ scheme. Furthermore, they proved that the numerical scheme is second-order convergence in the temporal direction and preserves the discrete maximum principle. In their subsequent work, Liao *et al.* [34] derived an asymptotically compatible energy of the TFACE and proved that the $L2-1\sigma$ scheme can preserve the energy dissipation law. Additionally, the authors in [46] constructed a finite difference scheme with the shifted fractional trapezoidal rule for the TFACE, and proved the scheme decays the discrete energy and preserves the maximum principle. Shen *et al.* [39] proposed a scheme by using the nonuniform time-stepping method in time and the finite difference method in space to solve the time-fractional Burgers' equation. The scheme is shown to preserve the variational energy dissipation law at the discrete level. Hou and Xu [13] presented an energy-dissipative scheme for the TFACE. Moreover, an energy-decaying variable-step L1 finite difference scheme to solve the time-fractional Swift-Hohenberg model was established in [47]. Most of the results focus on time-fractional phase-field models. A few numerical results were found on the time-fractional incompressible flow.

Recently, Gao *et al.* [10] presented an energy-dissipative method for TFNSE. To the best of our knowledge, it is the first energy-decaying scheme for the time-fractional incompressible flow. However, the theoretical and numerical results were limited to two-dimensional problems. Furthermore, the convergence results were obtained under some restrictions on the initial value. Due to the non-locality of the problem, the numerical scheme becomes time-consuming and requires significant computational storage, especially in long-time simulations. To overcome the difficulties, the sum-of-exponentials (SOEs) approximations have been widely adopted to accelerate the evaluation of convolution integrals, see [16,29,35]. Jiang *et al.* [17] first proposed a fast evaluation of the Caputo fractional derivative by applying the SOEs approximation for the kernel $t^{-\alpha}$ in the time discretization. This method reduces the number of nodes to be stored from M to $\mathcal{P}$, where $\mathcal{P}(\ll M)$ represents the number of exponentials needed, and M denoted the number of time-discrete grids. Inspired by Jiang's work, we further develop the SOEs technique to enhance the computational efficiency of our scheme, particularly for long-time simulations and higher-dimensional problems.

In this paper, we aim to overcome the above difficulties and then present a high-performance scheme to solve TFNSE. The highlights of the paper are as follows:

- The scheme is developed by taking both the initial layer and the energy-dissipative property into account. It is shown that the scheme can overcome the difficulties in dealing with the initial layer and mimic the energy dissipation at the discrete level.

- Optimal error estimates of the scheme in temporal direction are obtained for both two- and three-dimensional cases. It is shown that the temporal convergence rate of the numerical scheme is 2.

- A fast algorithm is applied to accelerate the computations. Numerical experiments are given to confirm the effectiveness and high efficiency of the scheme.

The rest of the paper is organized as follows. In Section 2, we construct a fully-discrete scheme for TFNSE by using nonuniform $L2-1\sigma$ approximation in time and the Fourier spectral method in space. The theoretical results and the implementation of the scheme are also presented. The theoretical results are rigorously proved in Section 3. In Section 4, several representative numerical experiments illustrate the high efficiency and effectiveness of the scheme. In Section 5, some conclusions and remarks are given.

Throughout the paper, we use C, C_u, C_τ to represent positive constants. Such representations could take different values. In addition, vector-valued spaces and vectors are denoted by boldface letters.

2. The Fully-discrete Scheme and Main Theoretical Results

The fully discrete numerical scheme and its corresponding fast version will be established in this section. Then, the main theoretical results will be presented. To start with, we denote

$$H_p^k(\Omega) = \{v \in L^2(\Omega) : D^j v \in L^2(\Omega),\ D^j v \text{ is periodic, for } |j| = 1, 2, \ldots, k\},$$

and define the vector-valued space $\mathbf{H}_p^k(\Omega)=[H_p^k(\Omega)]^d$, where $D^j=(\partial_{x_1})^{j_1}\ldots(\partial_{x_d})^{j_d}, j_1,\ldots,j_d\geq 0$ denotes differentiation of $\mathbf{x}$ with an arbitrary order $|j|$, where $|j| = j_1+\cdots+j_d$. The norm and

the semi-norm of the above space are defined by

$$\|v\|_k = \left(\sum_{|j|\le k} \|D^j v\|^2 \right)^{\frac{1}{2}}, \quad |v|_k = \left(\sum_{|j|=k} \|D^j v\|^2 \right)^{\frac{1}{2}}.$$

We set $\mathbf{H}_p^0(\Omega) = \mathbf{L}^2(\Omega)$, denote

$$\mathbf{L}_0^2(\Omega) = \left\{ \mathbf{u} \in \mathbf{L}^2(\Omega) : \int_\Omega \mathbf{u} d\mathbf{x} = 0 \right\},$$

and define the subset of $\mathbf{L}_0^2(\Omega), \mathbf{H}_p^1(\Omega)$ as

$$\mathbf{H} = \big\{ \mathbf{u} \in \mathbf{L}_0^2(\Omega) : \nabla \cdot \mathbf{u} = 0 \big\}, \quad \mathbf{V} = \big\{ \mathbf{u} \in \mathbf{H}_p^1(\Omega) : \nabla \cdot \mathbf{u} = 0 \big\}.$$

As in [37], we define

$$C_\kappa^m\big((0,T]\big) := \Big\{ \mathbf{v} \,\Big|\, \mathbf{v} \in C^m\big((0,T]\big) \bigcap C([0,T]) \text{ and } \big|\partial_t^l \mathbf{v}\big| \le C_{\mathbf{v}}(1 + t^{\kappa - l}) \text{ for } l = 1, \ldots, m \text{ with } 0 \le t \le T \Big\},$$

where $\kappa \in (0,1) \cup (1,2)$ is a regularity parameter.

2.1. Spatial discretization by the Fourier spectral method

We present a detailed spatial discretization for the two-dimensional TFNSE and take $\Omega = [0, L_x) \times [0, L_y)$ for simplicity. Spatial discretization in the three-dimensional case can be achieved similarly. Let $h_x = L_x/N_x$ and $h_y = L_y/N_y$ be spatial step-sizes, where N_x, N_y are positive even integers. Denote the Fourier approximation space by

$$S_N = \left\{ e^{\mathrm{i}\frac{2\pi j}{L_x}x} e^{\mathrm{i}\frac{2\pi k}{L_y}y} \,\middle|\, -\frac{N_x}{2} \le j \le \frac{N_x}{2} - 1,\ -\frac{N_y}{2} \le k \le \frac{N_y}{2} - 1 \right\},$$

where $j, k \in \mathbb{Z}$ and $\mathbf{i} = \sqrt{-1}$. The corresponding vector-valued space is defined as $\mathbf{S}_N$. The velocity $\mathbf{u} = (u_1, u_2)^\top$ and the pressure p can be approximated as

$$u_l(x,y,t) \approx u_{l,N}(t) = \sum_{j=-N_x/2}^{N_x/2-1} \sum_{k=-N_y/2}^{N_y/2-1} u_{l,j,k}(t) e^{\mathrm{i}\frac{2\pi j}{L_x}x} e^{\mathrm{i}\frac{2\pi k}{L_y}y}, \quad l = 1, 2,$$

$$p(x,y,t) \approx p_N(t) = \sum_{j=-N_x/2}^{N_x/2-1} \sum_{k=-N_y/2}^{N_y/2-1} p_{j,k}(t) e^{\mathrm{i}\frac{2\pi j}{L_x}x} e^{\mathrm{i}\frac{2\pi k}{L_y}y}.$$

Here we let $p_{0,0}(t) = 0$ so that the mean of p_N is 0, and define $\mathbf{u}_N = (u_{1,N}, u_{2,N})^\top$.

Define the L^2-orthogonal projection operator $\Pi_N : \mathbf{L}^2(\Omega) \to \mathbf{S}_N$ by [14]

$$(\Pi_N \mathbf{v} - \mathbf{v}, \boldsymbol{\phi}) = 0, \quad \forall\, \boldsymbol{\phi} \in \mathbf{S}_N, \quad \mathbf{v} \in \mathbf{L}^2(\Omega). \tag{2.1}$$

Then, the spatially discrete scheme for the TFNSE takes the form

$$\partial_t^\alpha \mathbf{u}_N - \nu \Delta \mathbf{u}_N + \Pi_N(\mathbf{u}_N \cdot \nabla \mathbf{u}_N) + \nabla p_N = 0, \tag{2.2}$$

$$\nabla \cdot \mathbf{u}_N = 0 \tag{2.3}$$

with initial value $\Pi_N(\mathbf{u}_0(x,y))$.

2.2. Temporal discretization with $L2-1\sigma$ approximation

We denote a time mesh as $0=t_0<t_1<t_2<\cdots<t_k<\cdots<t_M=T$ and the temporal step sizes as $\tau_k := t_k - t_{k-1}$, for $1\le k\le M$. Define the maximum temporal step size as $\tau=\max_{1\le k\le M}\tau_k$ and the time-step ratios as $r_k := \tau_k/\tau_{k-1}, \rho_k = 1/r_{k+1}, 2\le k\le M$. Let θ be an offset parameter and satisfy $\theta=\alpha/2$. To capture the initial layer, the following restrictions on the temporal meshes are needed [33].

M1. The maximum time-step ratio $\rho=\max_{2\le k\le M}\rho_k = 7/4$.

M2. There exists a constant $C_\delta>0$ such that $\tau_k/t_k \le C_\delta \tau_{k-1}/t_{k-1}$ for $2\le k\le M$ and $\tau_k\le C_\delta\tau\min\{1, t_k^{1-1/\delta}\}$ for $1\le k\le M$ with $t_k\le C_\delta t_{k-1}$.

For the grid function $\mathbf{w}=\{\mathbf{w}^k\,|\,1\le k\le M\}$, define

$$\nabla_\tau \mathbf{w}^k = \mathbf{w}^k-\mathbf{w}^{k-1},\quad \delta_\tau\mathbf{w}^k=\frac{\nabla_\tau\mathbf{w}^k}{\tau_k},\quad \mathbf{w}^{k-\theta}:=(1-\theta)\mathbf{w}^k+\theta\mathbf{w}^{k-1},\quad k\ge 1.$$

Based on the values at the time points t_{k-1} and t_k, we denote $\Pi_{1,k}\mathbf{u}$ as the linear interpolant of function $\mathbf{u}$. While, based on the values at the time points t_{k-1}, t_k, and t_{k+1}, we denote $\Pi_{2,k}\mathbf{u}$ as the quadratic interpolant of function $\mathbf{u}$. For $2\le k\le M$, it holds

$$(\Pi_{1,k}\mathbf{u})'(t)=\frac{\nabla_\tau\mathbf{u}^k}{\tau_k}, \tag{2.4}$$

$$(\Pi_{2,k}\mathbf{u})'(t)=\frac{\nabla_\tau\mathbf{u}^k}{\tau_k}+\frac{2(t-t_{k-1/2})}{\tau_{k+1}(\tau_k+\tau_{k+1})}\big(\nabla_\tau\mathbf{u}^{k+1}-r_{k+1}\nabla_\tau\mathbf{u}^k\big). \tag{2.5}$$

In each subinterval $[t_{k-1},t_k]$, we use (2.5). In the final subinterval $[t_{n-1},t_{n-\theta}]$, we use (2.4). Then, we obtain the $L2-1\sigma$ formula of Caputo derivative, that is

$$\begin{aligned}(D_\tau^\alpha\mathbf{v})^{n-\theta}&:=\int_{t_{n-1}}^{t_{n-\theta}}(\Pi_{1,k}\mathbf{v})'(s)\frac{(t_{n-\theta}-s)^{-\alpha}}{\Gamma(1-\alpha)}ds+\sum_{k=1}^{n-1}\int_{t_{k-1}}^{t_k}(\Pi_{2,k}\mathbf{v})'(s)\frac{(t_{n-\theta}-s)^{-\alpha}}{\Gamma(1-\alpha)}ds\\&=\sum_{k=1}^{n}A_{n-k}^{(n)}\nabla_\tau\mathbf{v}^k,\end{aligned} \tag{2.6}$$

where

$$t_{n-\theta}:=\theta t_{n-1}+(1-\theta)t_n,$$

and $A_{n-k}^{(n)}$ can be calculated by $A_0^{(1)}=a_0^{(1)}$ and

$$A_{n-k}^{(n)}=\begin{cases}a_0^{(n)}+\rho_{n-1}b_1^{(n)}, & k=n,\\ a_{n-k}^{(n)}+\rho_{k-1}b_{n-k+1}^{(n)}-b_{n-k}^{(n)}, & 2\le k\le n-1,\\ a_{n-1}^{(n)}-b_{n-1}^{(n)}, & k=1\end{cases}$$

with

$$\begin{aligned}a_0^{(n)}&=\frac{1}{\tau_n}\int_{t_{n-1}}^{t_{n-\theta}}\frac{(t_{n-\theta}-s)^{-\alpha}}{\Gamma(1-\alpha)}ds,\\ a_{n-k}^{(n)}&=\frac{1}{\tau_k}\int_{t_{k-1}}^{t_k}\frac{(t_{n-\theta}-s)^{-\alpha}}{\Gamma(1-\alpha)}ds,\\ b_{n-k}^{(n)}&=\frac{2}{\tau_k(\tau_k+\tau_{k+1})}\int_{t_{k-1}}^{t_k}\big(s-t_{k-\frac12}\big)\cdot\frac{(t_{n-\theta}-s)^{-\alpha}}{\Gamma(1-\alpha)}ds.\end{aligned}$$

The local consistency error can be written as

$$\mathcal{R}^{n-\theta} := \big(\partial_t^\alpha \mathbf{v}\big)(t_{n-\theta}) - \big(D_\tau^\alpha \mathbf{v}\big)^{n-\theta}. \tag{2.7}$$

Let $\mathbf{u}_N^n$ be the approximation of $\mathbf{u}_N$ at time point $t = t_n$. Applying (2.6) to approximate the time-fractional derivative ∂_t^α in (2.2), we present the fully-discrete numerical scheme for solving the TFNSE at the time point $t = t_{n-\theta}, 1 \le n \le M$,

$$\sum_{k=1}^{n} A_{n-k}^{(n)} \nabla_\tau \mathbf{u}_N^k - \nu\Delta \mathbf{u}_N^{n-\theta} + \Pi_N\big(\mathbf{u}_N^{n-\theta}\cdot\nabla \mathbf{u}_N^{n-\theta}\big) + \nabla p_N^{n-\theta} = 0, \tag{2.8}$$

$$\nabla\cdot \mathbf{u}_N^n = 0. \tag{2.9}$$

The initial condition is

$$\mathbf{u}_N^0 = \Pi_N \mathbf{u}_0(x,y). \tag{2.10}$$

Moreover, if taking the divergence on both sides of (2.8) and using the divergence-free condition (2.9), we can have

$$-\Delta p_N^{n-\theta} = \nabla\cdot \Pi_N\big(\mathbf{u}_N^{n-\theta}\cdot\nabla \mathbf{u}_N^{n-\theta}\big),$$

which implies

$$p_N^{n-\theta} = -(\Delta)^{-1}\nabla\cdot \Pi_N\big(\mathbf{u}_N^{n-\theta}\cdot\nabla \mathbf{u}_N^{n-\theta}\big). \tag{2.11}$$

Substituting (2.11) into (2.8), we can calculate $\mathbf{u}_N^{n-\theta}$ independently, i.e.

$$\sum_{k=1}^{n} A_{n-k}^{(n)} \nabla_\tau \mathbf{u}_N^k - \nu\Delta \mathbf{u}_N^{n-\theta} + \Pi_N\big(\mathbf{u}_N^{n-\theta}\cdot\nabla \mathbf{u}_N^{n-\theta}\big) - \nabla\big((\Delta)^{-1}\nabla\cdot \Pi_N\big(\mathbf{u}_N^{n-\theta}\cdot\nabla \mathbf{u}_N^{n-\theta}\big)\big) = 0.$$

With $\mathbf{u}_N^{n-\theta}$ known, $p_N^{n-\theta}$ can be calculated by (2.11).

2.3. Main results

As in [31], we introduce a family of complementary discrete convolution kernels $\{P_{n-k}^{(n)}\}_{k=1}^n$, which satisfies

$$\sum_{j=m}^{n} P_{n-j}^{(n)} A_{j-m}^{(j)} \equiv 1, \quad 1 \le m \le n \le N.$$

Such kernels can be given by

$$P_0^{(n)} := \frac{1}{A_0^{(n)}}, \quad P_j^{(n)} := \frac{1}{A_0^{(n-j)}} \sum_{k=0}^{j-1} \Big(A_{j-k-1}^{(n-k)} - A_{j-k}^{(n-k)}\Big) P_k^{(n)}, \quad 1 \le j \le n-1.$$

Next, we define the discrete energy as

$$\mathcal{E}_h\big(\mathbf{u}_N^n\big) = \frac{1}{2}\big\|\mathbf{u}_N^n\big\|^2 + \nu \sum_{m=1}^{n} P_{n-m}^{(n)} \big\|\nabla \mathbf{u}_N^{m-\theta}\big\|^2,$$

$$\mathcal{E}_h\big(\mathbf{u}_N^0\big) = \frac{1}{2}\big\|\mathbf{u}_N^0\big\|^2,$$

and the energy-dissipative property of the fully discrete scheme is presented below.

Theorem 2.1 (Energy Dissipation). *Let* $\mathbf{u}_0 \in \mathbf{V}\bigcap \mathbf{H}_p^3(\Omega)$. *Under the assumption* M1, *scheme* (2.8)-(2.10) *is unconditionally energy-dissipative, i.e.*

$$\mathcal{E}_h\big(\mathbf{u}_N^n\big) \le \mathcal{E}_h\big(\mathbf{u}_N^0\big), \quad 1 \le n \le M.$$

Below we present the boundedness and the error estimates of the numerical solution, and the proof will be left in the next section.

Theorem 2.2 (Boundedness). *Let* $\mathbf{u}_0 \in \mathbf{V}\bigcap \mathbf{H}_p^3(\Omega)$. *Under the assumption* M1, *the numerical solutions of scheme* (2.8)-(2.10) *satisfy*

$$\begin{aligned} &\big\|\mathbf{u}_N^n\big\| \le \big\|\mathbf{u}_N^0\big\|, \qquad 1 \le n \le M, \quad d = 3,\\ &\big\|\nabla\mathbf{u}_N^n\big\| \le \big\|\nabla\mathbf{u}_N^0\big\|, \quad 1 \le n \le M, \quad d = 2. \end{aligned}$$

Theorem 2.3 (Convergence Rates). *Suppose that* $\mathbf{u} \in \mathbf{C}([0,T], \mathbf{V}\bigcap \mathbf{H}_p^s(\Omega))\bigcap \mathbf{C}_\kappa^3([0,T], \mathbf{H}^1(\Omega))$, $\|\partial_t^\alpha \mathbf{u}\|_s \le C_u$, $\|\mathbf{u}\|_{k+2+2\alpha} \le C_u$ *with integer* $s \ge 3, k \ge 0$, *and the assumptions* M1-M2 *hold. Then, it holds that*

$$\big\|\mathbf{u}(t_n) - \mathbf{u}_N^n\big\| \le 2E_\alpha\big(C_\nu t_n^\alpha\big) \cdot \big(C_u C_\delta \tau^{\min\{2,\kappa\delta\}} + N^{-m}\big),$$

whenever $\tau \le 1/\sqrt[\alpha]{11\Gamma(2-\alpha)C_\nu}$, *where*

$$E_\alpha(z) = \sum_{k=0}^{\infty} \frac{z^k}{\Gamma(\alpha k + 1)}.$$

2.4. An accelerated algorithm

In this subsection, we present a fast version of the fully-discrete scheme (2.8)-(2.10) to accelerate the computation.

We split (2.6) into two parts

$$\begin{aligned} I &= \int_{t_{n-1}}^{t_{n-\theta}} (\Pi_{1,k}\mathbf{v})'(s) \frac{(t_{n-\theta}-s)^{-\alpha}}{\Gamma(1-\alpha)} ds,\\ II &= \sum_{k=1}^{n-1} \int_{t_{k-1}}^{t_k} (\Pi_{2,k}\mathbf{v})'(s) \frac{(t_{n-\theta}-s)^{-\alpha}}{\Gamma(1-\alpha)} ds. \end{aligned}$$

The first part is approximated by

$$I \approx \frac{\nabla_\tau \mathbf{u}^n}{\tau_n} \int_{t_{n-1}}^{t_{n-\theta}} \frac{(t_{n-\theta}-s)^{-\alpha}}{\Gamma(1-\alpha)} ds := a_0^{(n)} \nabla_\tau \mathbf{u}^n, \tag{2.12}$$

and the second part can be accelerated from an efficient sum-of-exponentials approximation for the kernel $t^{-\alpha}$. Suppose $\mu = \min_{1\le k\le M} \tau_k$ and ϵ as the absolute error, we have the following lemma.

Lemma 2.1 ([17, Theorem 2.1]). *For the given parameters* α, ϵ, μ *and* T, *one can find a family of points* s_i *and weights* $\omega_i : (i = 1, 2, \ldots, \mathcal{P})$ *such that*

$$\left| t^{-\alpha} - \sum_{i=1}^{\mathcal{P}} \omega_i e^{-s_i t} \right| \le \epsilon, \quad \forall\, t \in [\mu, T],$$

where the total number $\mathcal{P}$ *of exponentials needed is of order*

$$\mathcal{P} = \mathcal{O}\left(\left(\log\frac{T}{\mu} + \log(\log\epsilon^{-1})\right)\log\epsilon^{-1} + \big(\log\mu^{-1} + \log(\log\epsilon^{-1})\big)\log\mu^{-1}\right).$$

As in [17], the SOEs method is applied to approximate $t^{-\alpha}$. The second part is calculated by

$$\begin{aligned} II &\approx \frac{1}{\Gamma(1-\alpha)} \sum_{i=1}^{\mathcal{P}} \sum_{k=1}^{n-1} \int_{t_{k-1}}^{t_k} (\Pi_{2,k} v)'(s) w_i e^{-s_i(t_{n-\theta}-s)} ds \\ &= \frac{1}{\Gamma(1-\alpha)} \sum_{i=1}^{\mathcal{P}} \Bigg(\int_{t_{n-2}}^{t_{n-1}} (\Pi_{2,n-1} v)'(s) w_i e^{-s_i(t_{n-\theta}-s)} ds \\ &\qquad + \sum_{k=1}^{n-2} \int_{t_{k-1}}^{t_k} (\Pi_{2,k} v)'(s) w_i e^{-s_i(t_{n-\theta}-t_{n-1-\theta}+t_{n-1-\theta}-s)} ds \Bigg) \\ &= \frac{1}{\Gamma(1-\alpha)} \sum_{i=1}^{\mathcal{P}} \int_{t_{n-2}}^{t_{n-1}} (\Pi_{2,n-1} v)'(s) w_i e^{-s_i(t_{n-\theta}-s)} ds + e^{-s_i \tau_{n-\theta}} H_i(t_{n-2}), \end{aligned} \tag{2.13}$$

where $H_i(t_0) = 0$, and

$$H_i(t_{n-1}) = \sum_{k=1}^{n-1} \int_{t_{k-1}}^{t_k} (\Pi_{2,k} v)'(s) w_i e^{-s_i(t_{n-\theta}-s)} ds.$$

Combining (2.12) and (2.13), we get the fast nonuniform $L2-1\sigma$ approximation

$$\left({}^F D_\tau^\alpha \mathbf{u}\right)^{n-\theta} = \sum_{k=1}^{n} B_{n-k}^{(n)} \nabla_\tau \mathbf{u}^k \tag{2.14}$$

with

$$B_{n-k}^{(n)} = \begin{cases} a_0^{(n)} + \sum_{i=1}^{\mathcal{P}} \rho_{n-1} \hat{b}_1^{(n)}, & k = n, \\ \sum_{i=1}^{\mathcal{P}} e^{-s_i(t_{n-\theta}-t_{k+1-\theta})} \left(\hat{a}_{n-k}^{(k+1)} + e^{-s_i \tau_{k+1-\theta}} \rho_{k-1} \hat{b}_{n-k+1}^{(k)} - \hat{b}_{n-k}^{(k+1)} \right), & 2 \le k \le n-1, \\ \sum_{i=1}^{\mathcal{P}} e^{-s_i(t_{n-\theta}-t_{2-\theta})} \left(\hat{a}_{n-1}^{(2)} - \hat{b}_{n-1}^{(2)} \right), & k = 1, \end{cases}$$

where

$$\begin{aligned} \hat{a}_{n-k}^{(k+1)} &= \frac{\omega_i}{\tau_k \Gamma(1-\alpha)} \int_{t_{k-1}}^{t_k} e^{-s_i(t_{k+1-\theta}-s)} ds, \\ \hat{b}_{n-k}^{(k+1)} &= \frac{2\omega_i}{\tau_k(\tau_k+\tau_{k+1})\Gamma(1-\alpha)} \int_{t_{k-1}}^{t_k} (s - t_{k-\frac{1}{2}}) e^{-s_i(t_{k+1-\theta}-s)} ds. \end{aligned}$$

Using (2.14) to approximate the time-fractional derivative ∂_t^α in (2.2), we obtain the fast version of (2.8)-(2.10). Moreover, (2.14) only requires $\mathcal{O}(\log^2 M)$ storage and $\mathcal{O}(M \log^2 M)$ computational cost.

3. Proof of the Theoretical Results

In this section, we will prove the main theoretical results rigorously.

3.1. Preliminary

We first define a trilinear form

$$b(\mathbf{v},\mathbf{u},\mathbf{w})=\int_\Omega(\mathbf{v}\cdot\nabla)\mathbf{u}\cdot\mathbf{w}d\mathbf{x},$$

which satisfies, as pointed out in [14],

$$b(\mathbf{v},\mathbf{u},\mathbf{w})=-b(\mathbf{v},\mathbf{w},\mathbf{u}),\quad \forall\,\mathbf{u}\in\mathbf{H},\quad \mathbf{v},\mathbf{w}\in\mathbf{H}_p^1(\Omega),\tag{3.1}$$

and when $d=2$,

$$b(\mathbf{v},\mathbf{w},\Delta\mathbf{w})=0,\quad \forall\,\mathbf{v}\in\mathbf{H},\quad \mathbf{w}\in\mathbf{H}_p^1(\Omega).\tag{3.2}$$

Besides, the following embedding inequality holds [1, 2]:

$$\|\mathbf{v}\|_{L^l}\le C\|\mathbf{v}\|_{H^1},\quad 1\le l\le 6.\tag{3.3}$$

Some important lemmas are stated below, which play an important role in the subsequence analysis.

Lemma 3.1 ([23]). *For any $0\le k\le s$, there exists a constant C such that*

$$\|\Pi_N\mathbf{v}-\mathbf{v}\|_k\le C\|\mathbf{v}\|_s N^{k-s},\quad \forall\,\mathbf{v}\in\mathbf{H}_p^s(\Omega).$$

Lemma 3.2 ([33]). *Under the assumption* M1*, the discrete kernels $A_{n-k}^{(n)}, 1\le k\le n-1$ have the following properties:*

(I) The first kernel $A_0^{(n)}$ can be bounded by

$$A_0^{(n)}\le\frac{24}{11\pi}\int_{t_{n-1}}^{t_n}\frac{(t_n-s)^{-\alpha}}{\Gamma(1-\alpha)}ds,$$

and there is a constant $\pi_A>0$, so that $A_{n-k}^{(n)}$ are bounded by

$$A_{n-k}^{(n)}\ge\frac{1}{\pi_A\tau_k}\int_{t_{k-1}}^{t_k}\frac{(t_n-s)^{-\alpha}}{\Gamma(1-\alpha)}ds,\quad 1\le k\le n,$$

where $\pi_A=11/4$.

(II) The first kernel $A_0^{(n)}$ is appropriately larger than the second one,

$$\frac{1-2\theta}{1-\theta}A_0^{(n)}-A_1^{(n)}>0,\quad n\ge 2.$$

(III) The discrete kernels $A_{n-k}^{(n)}$ are monotone and satisfy

$$A_{n-k-1}^{(n)}-A_{n-k}^{(n)}\ge(1+\rho_k)b_{n-k}^{(n)}+\frac{1}{5\tau_k}\int_{t_{k-1}}^{t_k}(t_k-s)\frac{(t_{n-\theta}-s)^{-1-\alpha}}{\Gamma(\alpha)}ds.$$

Lemma 3.3 ([31, Lemma 4.1]). *Let the assumption* M1 *hold and fix the parameter $\theta\in[0,1)$. Then the sequence $\{\mathbf{u}^k\}_{k=0}^n$ in $\mathbf{L}^2(\Omega)$ satisfies*

$$\sum_{k=1}^n A_{n-k}^{(n)}\nabla_\tau(\|\mathbf{u}^k\|^2)\le 2\big(D_\tau^\alpha\mathbf{u}\big)^{n-\theta},u^{n-\theta}\big)-\xi_n(\theta^{(n)}-\theta)\big\|\big(D_\tau^\alpha\mathbf{u}\big)^{n-\theta}\big\|^2$$

for $1 \le n \le M$, *where* $0 < \xi_n < 1/A_0^{(n)}$ *and* $0 < \theta^{(n)} < 1/2$ *are given by*

$$\xi_n = \frac{2A_0^n - A_1^{(n)}}{A_0^{(n)}\big(A_0^{(n)} - A_1^{(n)}\big)}, \quad \theta^{(n)} := \frac{A_0^{(n)} - A_1^{(n)}}{2A_0^{(n)} - A_1^{(n)}} < \frac{1}{2}.$$

Lemma 3.4 ([33, Lemma 3.6]). *Assume that* $\mathbf{u} \in \mathbf{C}^3((0,T])$, *and there exists a positive constant* C_u *such that*

$$\left\| \frac{\partial^3 \mathbf{u}}{\partial t^3}(t) \right\| \le C_u(1 + t^{\kappa-3}), \quad 0 < t \le T$$

with the regularity parameter $\kappa \in (0,1) \cup (1,2)$. *Under the assumption* M1, *the global consistency error* (2.7) *satisfies, for* $1 \le n \le M$,

$$\sum_{k=1}^{n} P_{n-k}^{(n)} |\mathcal{R}^{n-\theta}| \le C_u \left(\frac{\tau_1^\kappa}{\kappa} + t_1^{\kappa-3}\tau_2^3 + \frac{1}{1-\alpha} \max_{2 \le k \le n} \frac{t_k^\alpha t_{k-1}^{\kappa-3} \tau^3}{\tau_{k-1}^\alpha} \right).$$

Lemma 3.5 ([37, Theorem 2.3]). *Let* $(\xi^n)_{n=1}^M, (\eta^n)_{n=1}^M$, *and* $(\lambda_l)_{l=0}^{M-1}$ *be given non-negative sequences. We assume further that there exists a constant* Λ (*independent of the step sizes*) *such that*

$$\Lambda \ge \sum_{l=0}^{M-1} \lambda_l,$$

and that the maximum step size satisfies

$$\tau \le \sqrt[\alpha]{\frac{1}{2\pi_A \Lambda \Gamma(2-\alpha)}}.$$

For any non-negative sequence $(u^k)_{k=0}^N$ *satisfying*

$$\sum_{k=1}^{n} A_{n-k}^{(n)} \nabla_\tau (u^k)^2 \le \sum_{k=1}^{n} \lambda_{n-k} (u^k)^2 + u^n \xi^n + (\eta^n)^2, \quad 1 \le n \le M,$$

it holds that, for $1 \le n \le M$,

$$u^n \le 2E_\alpha\big(2\max\{1,\rho\}\pi_A \Lambda t_n^\alpha\big) \left(u^0 + \max_{1 \le k \le n} \sum_{j=1}^{k} P_{k-j}^{(k)} \xi^j + \sqrt{\pi_A \Gamma(1-\alpha)} \max_{1 \le k \le n} \left\{ t_k^{\frac{\alpha}{2}} \eta^k \right\} \right).$$

3.2. Proof of Theorem 2.1

Taking the inner product of (2.8) with $\mathbf{u}_N^{n-\theta}$, we can get

$$\left(\sum_{k=1}^{n} A_{n-k}^{(n)} \nabla_\tau \mathbf{u}_N^k, \mathbf{u}_N^{n-\theta} \right) + \nu \big\| \nabla \mathbf{u}_N^{n-\theta} \big\|^2 + \big(\Pi_N \big(\mathbf{u}_N^{n-\theta} \cdot \nabla \mathbf{u}_N^{n-\theta} \big), \mathbf{u}_N^{n-\theta} \big) + \big(\nabla p_N^{n-\theta}, \mathbf{u}_N^{n-\theta} \big) = 0.$$

By using (2.1) and (3.1), we have

$$\big(\Pi_N \big(\mathbf{u}_N^{n-\theta} \cdot \nabla \mathbf{u}_N^{n-\theta} \big), \mathbf{u}_N^{n-\theta} \big) = \big(\mathbf{u}_N^{n-\theta} \cdot \nabla \mathbf{u}_N^{n-\theta}, \mathbf{u}_N^{n-\theta} \big) = 0.$$

Since

$$\big(\nabla p_N^{n-\theta}, \mathbf{u}_N^{n-\theta} \big) = -\big(p_N^{n-\theta}, \nabla \cdot \mathbf{u}_N^{n-\theta} \big),$$

and (2.9), we can get

$$\left(\left(D_\tau^\alpha \mathbf{u}_N\right)^{n-\theta}, \mathbf{u}_N^{n-\theta}\right) + \nu\left\|\nabla \mathbf{u}_N^{n-\theta}\right\|^2 = 0.$$

From Lemma 3.3, we have

$$\frac{1}{2}\left(D_\tau^\alpha \|\mathbf{u}_N\|^2\right)^{n-\theta} + \nu\left\|\nabla \mathbf{u}_N^{n-\theta}\right\|^2 \leq 0. \tag{3.4}$$

From the definition of kernels $P_{n-j}^{(n)}$, we have $P_0^{(n)} > 0$. Then, from the iterative procedure and (III) in Lemma 3.2, we can get $P_j^{(n)} \geq 0, 1 \leq j \leq n-1$. Multiplying both sides of (3.4) by $P_{m-n}^{(m)}$ and summing n from 1 to m, we arrive at

$$\sum_{n=1}^{m} P_{m-n}^{(m)} \sum_{k=1}^{n} A_{n-k}^{(n)} \nabla_\tau \left(\left\|\mathbf{u}_N^k\right\|\right)^2 + 2\nu \sum_{n=1}^{m} P_{m-n}^{(m)} \left\|\nabla \mathbf{u}_N^{n-\theta}\right\|^2 \leq 0.$$

From

$$\sum_{j=m}^{n} P_{n-j}^{(n)} A_{j-m}^{(j)} \equiv 1,$$

we can get

$$\left\|\mathbf{u}_N^m\right\|^2 - \left\|\mathbf{u}_N^0\right\|^2 = \sum_{k=1}^{m} \nabla_\tau \left\|\mathbf{u}_N^k\right\|^2 = \sum_{k=1}^{m} \sum_{n=k}^{m} P_{m-n}^{(m)} A_{n-k}^{(n)} \nabla_\tau \left\|\mathbf{u}_N^n\right\|^2,$$

which implies that

$$\frac{1}{2}\left\|\mathbf{u}_N^m\right\|^2 + \nu \sum_{n=1}^{m} P_{m-n}^{(m)} \left\|\nabla \mathbf{u}_N^{n-\theta}\right\|^2 \leq \frac{1}{2}\left\|\mathbf{u}_N^0\right\|^2.$$

We finish the proof. □

3.3. Proof of Theorem 2.2

We will give the theoretical analysis of the boundedness of $\|\mathbf{u}_N^n\|_{H^1}$ rigorously. And the bound in L^2-norm can be derived similarly. Taking the inner product of (2.8) with $-\Delta \mathbf{u}_N^{m-\theta}$, we have

$$\begin{aligned}&\left(\sum_{k=1}^{m} A_{m-k}^{(m)} \nabla_\tau \left(\nabla \mathbf{u}_N^k\right), \nabla \mathbf{u}_N^{m-\theta}\right) + \nu\left\|\Delta \mathbf{u}_N^{m-\theta}\right\|^2 \\ &\quad - b\left(\mathbf{u}_N^{m-\theta}, \mathbf{u}_N^{m-\theta}, \Delta \mathbf{u}_N^{m-\theta}\right) - \left(p_N^{m-\theta}, \nabla \cdot \left(\Delta \mathbf{u}_N^{m-\theta}\right)\right) = 0.\end{aligned}$$

By using (3.2), we have

$$\left(\sum_{k=1}^{m} A_{m-k}^{(m)} \nabla_\tau \left(\nabla \mathbf{u}_N^k\right), \nabla \mathbf{u}_N^{m-\theta}\right) + \nu\left\|\Delta \mathbf{u}_N^{m-\theta}\right\|^2 = 0.$$

By using Lemma 3.3, we can obtain

$$\sum_{k=1}^{m} A_{m-k}^{(m)} \nabla_\tau \left\|\nabla \mathbf{u}_N^k\right\|^2 \leq 0.$$

Replace the index m with j, then multiply by $P_{n-j}^{(n)}$ and sum j from 1 to n, we can obtain

$$\sum_{j=1}^{n} P_{n-j}^{(n)} \sum_{k=1}^{j} A_{j-k}^{(j)} \nabla_\tau \|\nabla \mathbf{u}_N^k\|^2 \leq 0.$$

Since the left-hand side of the above inequality can be rewritten as

$$\begin{aligned}
&\sum_{j=1}^{n} P_{n-j}^{(n)} \sum_{k=1}^{j} A_{j-k}^{(j)} \nabla_\tau \|\nabla \mathbf{u}_N^k\|^2 \\
&= \sum_{k=1}^{n} \left(\sum_{j=k}^{n} P_{n-j}^{(n)} A_{j-k}^{(j)} \right) \nabla_\tau \|\nabla \mathbf{u}_N^k\|^2 \\
&= \sum_{k=1}^{n} \nabla_\tau \|\nabla \mathbf{u}_N^k\|^2 = \|\nabla \mathbf{u}_N^n\|^2 - \|\nabla \mathbf{u}_N^0\|^2,
\end{aligned}$$

we arrive

$$|\mathbf{u}_N^n|_1 \leq |\mathbf{u}_N^0|_1.$$

We can derive the bound of $\|\mathbf{u}_N^n\|_{L^2}$ from the energy stability. □

3.4. Proof of Theorem 2.3

In the following, we let $\mathbf{u}^n = \mathbf{u}(t_n), p^n = p(t_n)$ and define

$$\mathbf{e}^n = \mathbf{u}^n - \mathbf{u}_N^n, \quad \mathbf{e}_\Pi^n = \mathbf{u}^n - \Pi_N \mathbf{u}^n, \quad \mathbf{e}_N^n = \Pi_N \mathbf{u}^n - \mathbf{u}_N^n, \quad \mathbf{e}^n = \mathbf{e}_\Pi^n + \mathbf{e}_N^n, \quad e_p^n = p^n - p_N^n.$$

Obviously, for any $\mathbf{v} \in \mathbf{S}_N$, it holds that

$$\left(\sum_{k=1}^{n} A_{n-k}^{(n)} \nabla_\tau \mathbf{u}^k, \mathbf{v} \right) + \nu(\nabla \mathbf{u}^{n-\theta}, \nabla \mathbf{v}) + (\mathbf{u}^{n-\theta} \cdot \nabla \mathbf{u}^{n-\theta}, \mathbf{v}) + (\nabla p^{n-\theta}, \mathbf{v}) = (\mathcal{R}^{n-\theta}, \mathbf{v}), \quad (3.5)$$

$$\left(\sum_{k=1}^{n} A_{n-k}^{(n)} \nabla_\tau \mathbf{u}_N^k, \mathbf{v} \right) + \nu\big(\nabla \mathbf{u}_N^{n-\theta}, \nabla \mathbf{v}\big) + \big(\Pi_N \big(\mathbf{u}_N^{n-\theta} \cdot \nabla \mathbf{u}_N^{n-\theta}\big), \mathbf{v}\big) + \big(\nabla p_N^{n-\theta}, \mathbf{v}\big) = 0. \quad (3.6)$$

Subtracting (3.6) from (3.5), we get

$$\begin{aligned}
&\left(\sum_{k=1}^{n} A_{n-k}^{(n)} \nabla_\tau \mathbf{e}^k, \mathbf{v} \right) + \nu(\nabla \mathbf{e}^{n-\theta}, \nabla \mathbf{v}) + \big(\mathbf{u}^{n-\theta} \cdot \nabla \mathbf{u}^{n-\theta} - \mathbf{u}_N^{n-\theta} \cdot \nabla \mathbf{u}_N^{n-\theta}, \mathbf{v}\big) \\
&\quad + \big(\nabla e_p^{n-\theta}, \mathbf{v}\big) = (\mathcal{R}^{n-\theta}, \mathbf{v}), \quad \forall\, \mathbf{v} \in \mathbf{S}_N. \qquad (3.7)
\end{aligned}$$

Let $\mathbf{v} = \mathbf{e}_N^{n-\theta}$ in (3.7), and we have

$$\begin{aligned}
&\left(\sum_{k=1}^{n} A_{n-k}^{(n)} \nabla_\tau \mathbf{e}_N^k, \mathbf{e}_N^{n-\theta} \right) + \nu \|\nabla \mathbf{e}_N^{n-\theta}\|^2 \\
&= \big(\mathcal{R}^{n-\theta}, \mathbf{e}_N^{n-\theta}\big) - \big(\mathbf{u}^{n-\theta} \cdot \nabla \mathbf{u}^{n-\theta} - \mathbf{u}_N^{n-\theta} \cdot \nabla \mathbf{u}_N^{n-\theta}, \mathbf{e}_N^{n-\theta}\big), \qquad (3.8)
\end{aligned}$$

where we have used (2.1) and $(e_p^{n-\theta}, \nabla \cdot \mathbf{e}_N^{n-\theta}) = 0$. We estimate the first term on the right-hand side of (3.8) by using the Cauchy-Schwarz inequality, that is,

$$\big(\mathcal{R}^{n-\theta}, \mathbf{e}_N^{n-\theta}\big) \leq \|\mathcal{R}^{n-\theta}\| \cdot \|\mathbf{e}_N^{n-\theta}\|. \quad (3.9)$$

Then, we calculate the second term on the right-hand side of (3.8) as

$$\begin{aligned}
&-\big(\mathbf{u}^{n-\theta}\cdot\nabla\mathbf{u}^{n-\theta}-\mathbf{u}_N^{n-\theta}\cdot\nabla\mathbf{u}_N^{n-\theta},\mathbf{e}_N^{n-\theta}\big)\\
&=-\big(\mathbf{u}_N^{n-\theta}\cdot\nabla\mathbf{e}^{n-\theta},\mathbf{e}_N^{n-\theta}\big)-\big(\mathbf{e}^{n-\theta}\cdot\nabla\mathbf{u}^{n-\theta},\mathbf{e}_N^{n-\theta}\big)\\
&=-\big(\mathbf{u}_N^{n-\theta}\cdot\nabla\mathbf{e}_N^{n-\theta},\mathbf{e}_N^{n-\theta}\big)-\big(\mathbf{u}_N^{n-\theta}\cdot\nabla\mathbf{e}_\Pi^{n-\theta},\mathbf{e}_N^{n-\theta}\big)\\
&\quad-\big(\mathbf{e}_N^{n-\theta}\cdot\nabla\mathbf{u}^{n-\theta},\mathbf{e}_N^{n-\theta}\big)-\big(\mathbf{e}_\Pi^{n-\theta}\cdot\nabla\mathbf{u}^{n-\theta},\mathbf{e}_N^{n-\theta}\big)\\
&\le\big\|\mathbf{u}_N^{n-\theta}\big\|_{L^2}\big\|\nabla\mathbf{e}_\Pi^{n-\theta}\big\|_{L^3}\big\|\mathbf{e}_N^{n-\theta}\big\|_{L^6}+\big\|\mathbf{e}_N^{n-\theta}\big\|_{L^2}\|\nabla\mathbf{u}^{n-\theta}\|_{L^3}\big\|\mathbf{e}_N^{n-\theta}\big\|_{L^6}\\
&\quad+\big\|\mathbf{e}_\Pi^{n-\theta}\big\|_{L^2}\|\nabla\mathbf{u}^{n-\theta}\|_{L^3}\big\|\mathbf{e}_N^{n-\theta}\big\|_{L^6}\\
&\le C(\epsilon)\big\|\mathbf{e}_\Pi^{n-\theta}\big\|_2^2+\epsilon\big\|\mathbf{e}_N^{n-\theta}\big\|_1^2+C(\epsilon)\big\|\mathbf{e}_N^{n-\theta}\big\|^2\\
&\quad+\epsilon\big\|\mathbf{e}_N^{n-\theta}\big\|_1^2+C(\epsilon)\big\|\mathbf{e}_\Pi^{n-\theta}\big\|_1^2+\epsilon\big\|\mathbf{e}_N^{n-\theta}\big\|_1^2,
\end{aligned}$$

where we have used the Cauchy-Schwarz inequality, (3.3) and the Hölder inequality. Then, by using Lemma 3.3, we can estimate the first term on the left-hand side of (3.8) as

$$\left(\sum_{k=1}^{n}A_{n-k}^{(n)}\nabla_\tau\mathbf{e}_N^k,\mathbf{e}_N^{n-\theta}\right)\ge\frac{1}{2}\sum_{k=1}^{n}A_{n-k}^{(n)}\nabla_\tau\big\|\mathbf{e}_N^k\big\|^2. \tag{3.10}$$

Combining (3.9)-(3.10), we have

$$\begin{aligned}
&\frac{1}{2}\sum_{k=1}^{n}A_{n-k}^{(n)}\nabla_\tau\big\|\mathbf{e}_N^k\big\|^2+\nu\big\|\nabla\mathbf{e}_N^{n-\theta}\big\|^2\\
&\le\|\mathcal{R}^{n-\theta}\|\cdot\big\|\mathbf{e}_N^{n-\theta}\big\|+C(\epsilon)\Big(\big\|\mathbf{e}_\Pi^{n-\theta}\big\|_1^2+\big\|\mathbf{e}_\Pi^{n-\theta}\big\|_2^2\Big)+C(\epsilon)\big\|\mathbf{e}_N^{n-\theta}\big\|^2+3\epsilon\big\|\mathbf{e}_N^{n-\theta}\big\|_1^2.
\end{aligned}$$

When $\epsilon<\nu/3$, we get

$$\sum_{k=1}^{n}A_{n-k}^{(n)}\nabla_\tau\big\|\mathbf{e}_N^k\big\|^2\le2\|\mathcal{R}^{n-\theta}\|\big\|\mathbf{e}_N^{n-\theta}\big\|+C(\epsilon)\big\|\mathbf{e}_N^{n-\theta}\big\|^2+C(\epsilon)\left(\big\|\mathbf{e}_\Pi^{n-\theta}\big\|_1^2+\big\|\mathbf{e}_\Pi^{n-\theta}\big\|_2^2\right).$$

Letting

$$v^n=\big\|\mathbf{e}_N^n\big\|,\quad\sum_{l=0}^{M-1}\lambda_l=C(\epsilon),\quad\Lambda=C(\epsilon),\quad\xi^n=2\|\mathcal{R}^{n-\theta}\|,\quad\eta^n=\big\|\mathbf{e}_\Pi^{n-\theta}\big\|_1+\big\|\mathbf{e}_\Pi^{n-\theta}\big\|_2$$

in Lemma 3.5, we arrive at

$$\begin{aligned}
\big\|\mathbf{e}_N^n\big\|\le2E_\alpha\big(2\max\{1,\rho\}\pi_A\Lambda t_n^\alpha\big)\cdot\Bigg[&C_u\left(\frac{\tau_1^\kappa}{\kappa}+t_1^{\kappa-3}\tau_2^3+\frac{1}{1-\alpha}\max_{2\le k\le n}\frac{t_k^\alpha t_{k-1}^{\kappa-3}\tau_k^3}{\tau_{k-1}^\alpha}\right)\\
&+\sqrt{\pi_A\Gamma(1-\alpha)}\max_{1\le k\le n}t_k^{\frac{\alpha}{2}}\eta^k\Bigg]
\end{aligned}$$

for $\tau<\sqrt[\alpha]{11\Gamma(2-\alpha)C(\epsilon)}$. From Lemma 3.2, we can get $\pi_A=11/4$. If the mesh assumption M2 holds, then $\tau_1\le C_\delta\tau^\delta$, and

$$\begin{aligned}
\frac{t_k^\alpha t_{k-1}^{\kappa-3}\tau_k^3}{\tau_{k-1}^\alpha}&\le C_\delta t_k^{\alpha+\kappa-3}\tau_k^{3-\alpha}\le C_\delta t_k^{\alpha+\kappa-3}\tau_k^{3-\alpha-\beta}\tau_k^\beta\\
&\le C_\delta t_k^{\kappa-3+\alpha}\tau_k^{3-\alpha-\beta}\tau^\beta\big(\min\big\{1,t_k^{1-\frac{1}{\delta}}\big\}\big)^\beta\\
&\le C_\delta t_k^{\kappa-\frac{\beta}{\delta}}\tau^\beta\left(\frac{\tau_k}{t_k}\right)^{3-\alpha-\beta}\le C_\delta\tau^\beta t_k^{\max\{0,\kappa-\frac{3-\alpha}{\delta}\}},
\end{aligned}$$

where $\beta := \min\{2, \kappa\delta\}, 2 \le k \le n$. Moreover, we have

$$t_{k-1}^{\kappa-2}\tau_k^2 \le C_\delta t_k^{\kappa-2}\tau_k^{2-\beta}\tau^\beta\big(\min\big\{1, t_k^{1-\frac{1}{\delta}}\big\}\big)^\beta \le C_\delta t_k^{\kappa-\frac{\beta}{\delta}}\tau^\beta\left(\frac{\tau_k}{t_k}\right)^{2-\beta} \le C_\delta\tau^\beta t_k^{\max\{0,\kappa-\frac{2}{\delta}\}},$$
$$t_1^{\kappa-3}\tau_2^3 \le C_\delta t_2^{\kappa-3}\tau_2^{3-\beta}\tau^\beta\big(\min\big\{1, t_2^{1-\frac{1}{\delta}}\big\}\big)^\beta \le C_\delta\tau^\beta t_2^{\kappa-\frac{\beta}{\delta}}\left(\frac{\tau_2}{t_2}\right)^{3-\beta} \le C_\delta\tau^\beta t_2^{\max\{0,\kappa-\frac{3}{\delta}\}}.$$

By noting that $t_k \le T$, the error can be estimated as

$$\big\|\mathbf{e}_N^n\big\| \le 2E_\alpha\big(C(\epsilon)t_n^\alpha\big)\cdot\big(C_uC_\delta\tau^{\min\{2,\kappa\delta\}} + N^{2-m}\big).$$

Finally, we can get

$$\|\mathbf{e}^n\| \le \big\|\mathbf{e}_\Pi^n\big\| + \big\|\mathbf{e}_N^n\big\| \le 2E_\alpha\big(C(\epsilon)t_n^\alpha\big)\cdot\big(C_uC_\delta\tau^{\min\{2,\kappa\delta\}} + N^{-m}\big).$$

This completes the proof. □

4. Numerical Experiments

This section presents several numerical examples to confirm the effectiveness of the proposed schemes. We define

$$\|\mathbf{E}_N\| = \big\|\mathbf{e}_N^M\big\|, \quad \|E_p\| = \big\|e_p^M\big\|,$$

where the errors are calculated at time point $t_M = T$. In the following, we only test the convergence orders by choosing $\delta = 2/\alpha$. Similar numerical experiments for different choices of δ can be found in [33, 34].

Example 4.1. We consider the following two-dimensional TFNSE:

$$\begin{cases}\partial_t^\alpha\mathbf{u} - \nu\Delta\mathbf{u} + \mathbf{u}\cdot\nabla\mathbf{u} + \nabla p = f(x,y,t),\\ \nabla\cdot\mathbf{u} = 0\end{cases} \tag{4.1}$$

with the following exact solutions:

$$\begin{aligned}u_1(x,y,t) &= (t^\alpha + t^2 + 1)\sin^2(x)\sin(2y),\\ u_2(x,y,t) &= -(t^\alpha + t^2 + 1)\sin(2x)\sin^2(y),\\ p(x,y,t) &= (t^\alpha + t^2 + 1)^2\cos(x)\sin(y)\end{aligned}$$

in domain $\Omega = (0, 2\pi)\times(0, 2\pi)$. The source term $f(x, y, t)$ is computed according to the exact solutions.

Convergence tests. We test the errors and convergence rates of the proposed scheme (2.8)-(2.10). We set $T = 1$, and the time grid nodes are calculated by $t_k = T(k/M)^\delta, 0 \le k \le M$. The spatial grid number is fixed as $N = 8$. Other parameters are fixed as $\nu = 1$, $\alpha = 0.4, 0.6, 0.8$ and $\kappa = \alpha$. The numerical results with different α for the velocity and the pressure are presented in Tables 4.1 and 4.2, respectively. The convergence orders of the velocity can reach 2, which are consistent with our theoretical results. Moreover, the convergence orders of the pressure can also lead to 2, which shows the effectiveness of our numerical schemes.

Energy evolution. We set $f(x, y, t) = 0$ and $T = 50$. The time interval is split into two parts. The first part is $[0, T_0]$ and time mesh is calculated as $t_k = T_0(k/N_0)^\delta, \delta = 2/\alpha$,

Table 4.1: Numerical results for $\|\mathbf{E}_N\|$ with $\delta = 2/\alpha, \nu = 1$, and $N = 8$ for Example 4.1.

M	$\alpha = 0.4$		$\alpha = 0.6$		$\alpha = 0.8$	
	Error	Order	Error	Order	Error	Order
8	7.94e-02	*	5.73e-02	*	4.29e-02	*
16	2.45e-02	1.70	1.56e-02	1.88	1.11e-02	1.95
32	6.70e-03	1.87	4.04e-03	1.95	2.80e-03	1.98
64	1.76e-03	1.93	1.03e-03	1.98	7.02e-04	1.99

Table 4.2: Numerical results for $\|E_p\|$ with $\delta = 2/\alpha, \nu = 1$, and $N = 8$ for Example 4.1.

M	$\alpha = 0.4$		$\alpha = 0.6$		$\alpha = 0.8$	
	Error	Order	Error	Order	Error	Order
8	3.08e-01	*	2.23e-01	*	1.67e-01	*
16	9.53e-02	1.69	6.09e-02	1.87	4.31e-02	1.95
32	2.61e-02	1.87	1.58e-02	1.95	1.09e-02	1.98
64	6.47e-03	2.01	4.01e-03	1.98	2.74e-03	1.99

$0 \le k \le N_0$ and $T_0 = 0.01, N_0 = 20$. The second part is $[T_0, T]$ and time mesh is calculated by the following adaptive time-stepping strategy [33]:

$$\tau_{ada} = \max\left\{\tau_{\min}, \frac{\tau_{\max}}{1 + \eta\|\nabla_\tau \mathcal{E}(\mathbf{u})\|^2}\right\} \tag{4.2}$$

with $\tau_{\min} = 10^{-2}, \tau_{\max} = 10^{-1}$ and $\eta = 10$. The viscosity is chosen as $\nu = 0.1$ and $\alpha = 0.4$, $0.6, 0.8$. The energy evolution of the above problem is presented in Fig. 4.1(a). Corresponding evolution of the step-sizes with different α are shown in Fig. 4.1(b). We can find that the numerical scheme fulfills the discrete energy dissipation for both large and small α. Furthermore, we also test the velocity divergence

$$D\big(\mathbf{u}_N^n\big) = \big|\partial_x u_{1,N}^n + \partial_y u_{2,N}^n\big|, \quad 1 \le n \le M \tag{4.3}$$

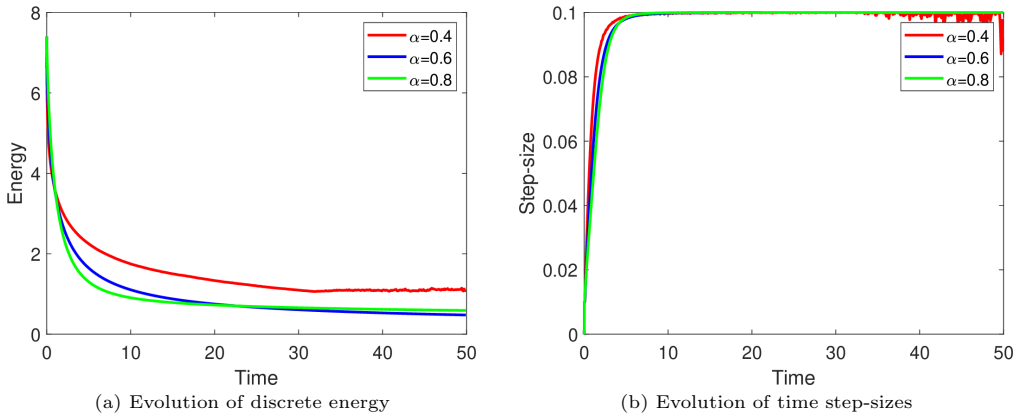

(a) Evolution of discrete energy (b) Evolution of time step-sizes

Fig. 4.1. Evolution of discrete energy (a) and time step-sizes (b) with $\alpha = 0.4, 0.6, 0.8$ for Example 4.1.

with different α in Fig. 4.2, where $\mathbf{u}_N^n = (u_{1,N}^n, u_{2,N}^n)^\top$. Such performances illustrate the stability and effectiveness of our scheme in the long-time simulation.

Then, we choose the Fourier modes as 128×128 to show the vorticity contours in Fig. 4.3. We choose time step-sizes by using (4.2), where we set $\tau_{\min} = 10^{-2}, \tau_{\max} = 10^{-1}$ and $\eta = 10$. The viscosity is set as $\nu = 0.0001$. In Fig. 4.3, we can observe the generation of four vortices that gradually rotate in an anti-clockwise direction.

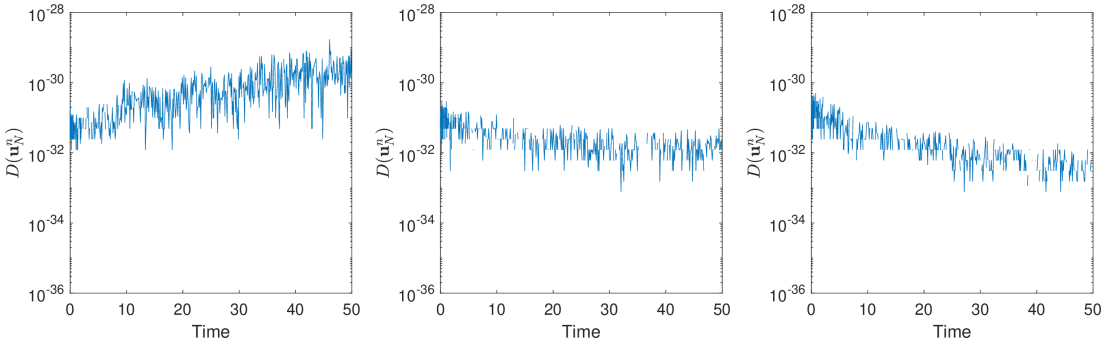

Fig. 4.2. Evolution of velocity divergence with different α: 0.4(left), 0.6(middle), 0.8(right) for Example 4.1.

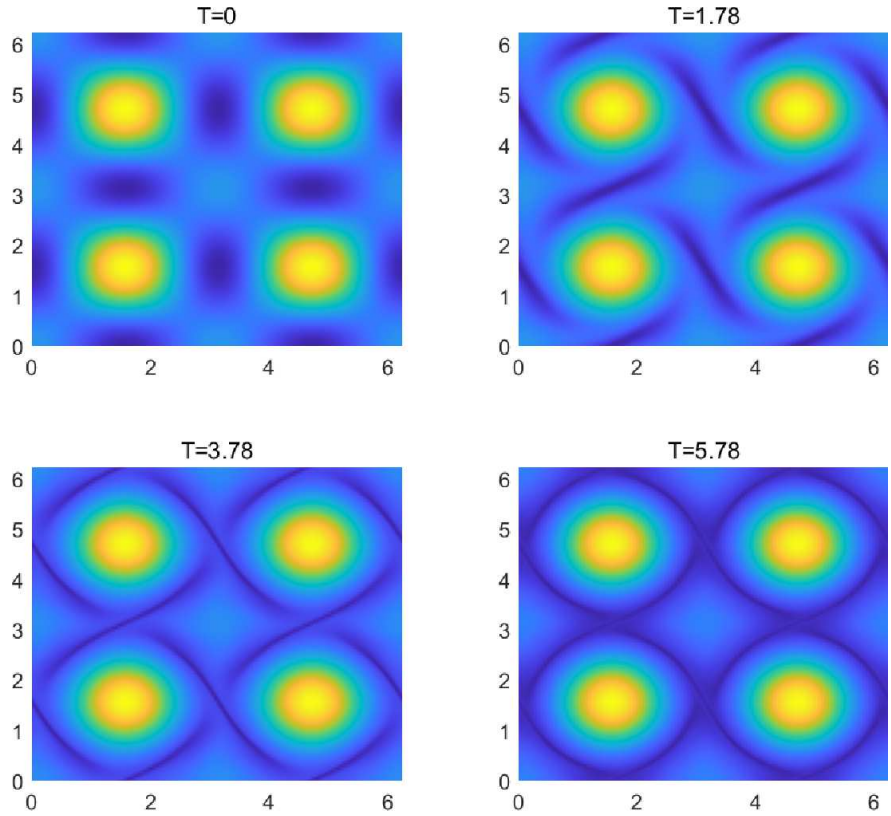

Fig. 4.3. Vorticity contours at $t = 0, 1.78, 3.78, 5.78$ with $\alpha = 0.8, \nu = 0.0001$ for Example 4.1.

Comparison of computation time. We compare the computational time of the nonuniform $L2-1\sigma$ scheme ($L2-1\sigma$) (2.8) and the fast nonuniform $L2-1\sigma$ scheme (F$L2-1\sigma$) (2.14) in Table 4.3. The spatial grid number is fixed as $N=8$, and the time grid nodes are calculated by $t_k = T(k/M)^\delta, \delta = 2, 0 \le k \le M$ with $T=1$. The viscosity is chosen to be 1. To calculate the weights w_i and points s_i, we define the time step as $\max\{10^{-14}, \min_{0\le k\le M}\tau_k\}$ and the error as $\epsilon = 10^{-8}$. From the calculation, the smaller the temporal step sizes, the more effective the fast numerical scheme.

Table 4.3: Computational time with $\delta = 2, \nu = 1$, and $N = 8$ for Example 4.1.

M	$\alpha = 0.4$		$\alpha = 0.6$		$\alpha = 0.8$	
	F$L2-1\sigma$	$L2-1\sigma$	F$L2-1\sigma$	$L2-1\sigma$	F$L2-1\sigma$	$L2-1\sigma$
8000	6.82s	99.45s	8.59s	107.5020s	7.16s	90.557s
16000	16.27s	465.55s	18.94s	425.43s	14.54s	361.17s
32000	35.99s	1702.28s	44.68s	1843.45s	30.72s	1438.33s
64000	69.70s	6790.50s	62.18s	7370.41s	61.44s	5742.22s

Example 4.2. We consider the following three-dimensional TFNSE:

$$\begin{cases} \partial_t^\alpha \mathbf{u} - \nu\Delta\mathbf{u} + \mathbf{u}\cdot\nabla\mathbf{u} + \nabla p = f(x,y,z,t), \\ \nabla\cdot\mathbf{u} = 0 \end{cases} \tag{4.4}$$

with the following exact solutions:

$$\begin{aligned} u_1(x,y,z,t) &= (t^2 + t^\alpha + 1)\sin(x)\cos(y)\cos(z), \\ u_2(x,y,z,t) &= (t^2 + t^\alpha + 1)\cos(x)\sin(y)\cos(z), \\ u_3(x,y,z,t) &= -2(t^2 + t^\alpha + 1)\cos(x)\cos(y)\sin(z), \\ p(x,y,z,t) &= (1 + t^\alpha + t^2)\sin(x)\sin(y)\sin(z) \end{aligned}$$

in domain $\Omega = (0, 2\pi)^3$. The source term $f(x,y,z,t)$ is computed according to the exact solutions.

Convergence tests. We set $T=1$ and $\nu=1$ to compute the numerical solutions. We define the temporal step size as $t_k = T(k/M)^\delta, 0 \le k \le M$. We fix the spatial grid number as $N=8$, the order of Caputo fractional derivative as $\alpha = 0.4, 0.6, 0.8$ and $\kappa = \alpha$. Then, we present the errors and convergence rates with different α in Tables 4.4 and 4.5 for the velocity and the pressure, respectively. The convergence orders of the velocity and the pressure can reach 2, which is consistent with our theoretical convergence results.

Energy evolution. We set $f \equiv 0$ and $T = 50$ to compute the numerical solutions. The time interval is split into two parts. The first part is $[0, T_0]$ and the time mesh is calculated as $t_k = T_0(k/N_0)^\delta, \delta = 2/\alpha, 0 \le k \le N_0$, with $T_0 = 0.01, N_0 = 20$. The second part is $[T_0, T]$ and time mesh is calculated by (4.2) with corresponding parameters chosen as $\tau_{\min} = 10^{-2}, \tau_{\max} = 10^{-1}$ and $\eta = 10$. The viscosity is set as 0.1 and $\alpha = 0.4, 0.6, 0.8$. The discrete energy evolution is presented in Fig. 4.4(a). The evolution of the step-sizes with different α is shown in Fig. 4.4(b). Then, we also compute the velocity divergence

$$D(\mathbf{u}_N^n) = \left|\partial_x u_{1,N}^n + \partial_y u_{2,N}^n + \partial_z u_{3,N}^n\right|, \quad 1 \le n \le M \tag{4.5}$$

Table 4.4: Numerical results for $\|\mathbf{E}_N\|$ with $\delta = 2/\alpha, \nu = 1$, and $N = 8$ for Example 4.2.

M	$\alpha = 0.4$		$\alpha = 0.6$		$\alpha = 0.8$	
	Error	Order	Error	Order	Error	Order
8	2.94e-01	*	2.10e-01	*	1.56e-01	*
16	9.06e-02	1.70	5.72e-02	1.87	4.03e-02	1.95
32	2.48e-02	1.87	1.48e-02	1.95	1.02e-02	1.98
64	6.65e-03	1.90	3.76e-03	1.98	2.56e-03	1.99

Table 4.5: Numerical results for $\|E_p\|$ with $\delta = 2/\alpha, \nu = 1$, and $N = 8$ for Example 4.2.

M	$\alpha = 0.4$		$\alpha = 0.6$		$\alpha = 0.8$	
	Error	Order	Error	Order	Error	Order
8	9.97e-01	*	7.12e-01	*	5.30e-01	*
16	3.08e-01	1.69	1.95e-01	1.87	1.37e-01	1.95
32	8.46e-02	1.87	5.05e-02	1.95	3.47e-02	1.98
64	2.13e-02	2.00	1.28e-02	1.98	8.73e-03	1.99

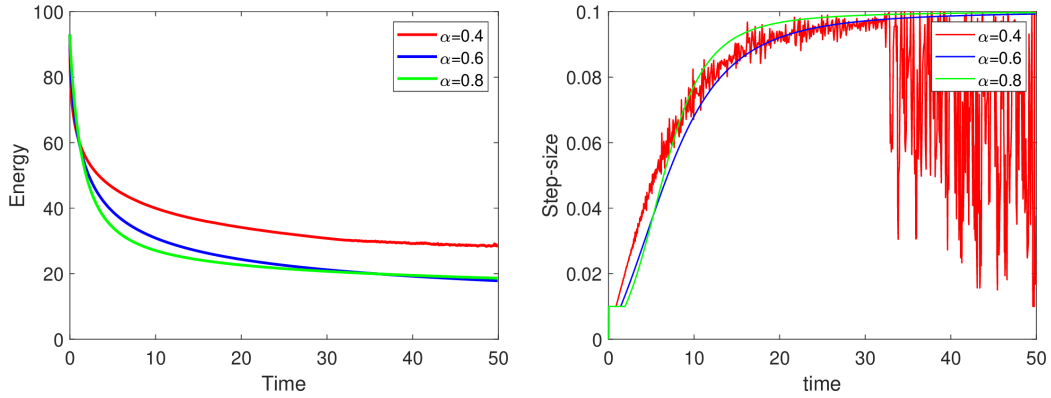

(a) Evolution of discrete energy (b) Evolution of time step-sizes

Fig. 4.4. Evolution of discrete energy (a) and time step-sizes (b) with $\alpha = 0.4, 0.6, 0.8$ for Example 4.2.

with different α in Fig. 4.5, where $\mathbf{u}_N^n = (u_{1,N}^n, u_{2,N}^n, u_{3,N}^n)^T$. Such performances show that the numerical scheme can preserve the discrete energy dissipation during the long-time simulations in the three-dimensional cases.

Comparison of computation time. We compare the computational time of the nonuniform $L2-1\sigma$ scheme ($L2-1\sigma$) (2.8) and the fast nonuniform $L2-1\sigma$ scheme (F$L2-1\sigma$) (2.14) in Table 4.6. The spatial grid number is fixed as $N = 8$, and the time grid nodes are calculated by $t_k = T(k/M)^\delta, \delta = 2, 0 \le k \le M$ in time interval $[0, 1]$. The viscosity is set as 1. To calculate the weights w_i and points s_i, we define the time step as $\max\{10^{-14}, \min_{0\le k\le M} \tau_k\}$ and the error as $\epsilon = 10^{-8}$. From the table, one can see the effectiveness and high efficiency of the fast scheme.

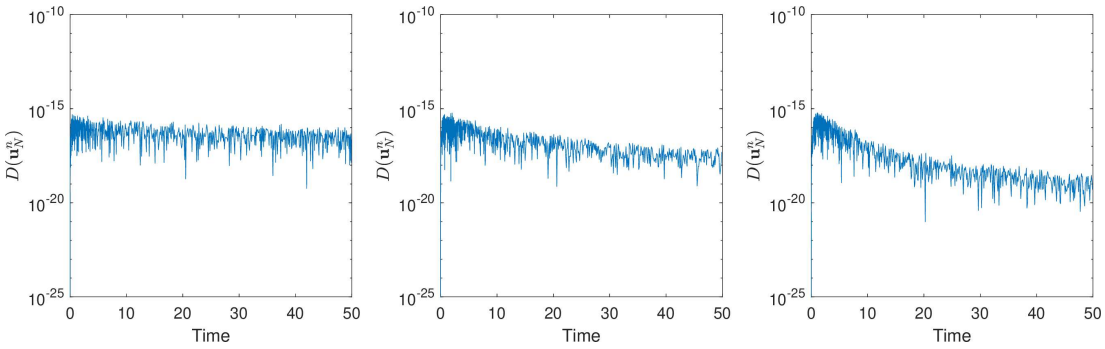

Fig. 4.5. Evolution of velocity divergence with different α: 0.4 (left), 0.6 (middle), 0.8 (right) for Example 4.2.

Table 4.6: Computational time with $\delta = 1, \nu = 1$, and $N = 8$ for Example 4.2.

M	$\alpha = 0.4$		$\alpha = 0.6$		$\alpha = 0.8$	
	F$L2-1\sigma$	$L2-1\sigma$	F$L2-1\sigma$	$L2-1\sigma$	F$L2-1\sigma$	$L2-1\sigma$
8000	31.62s	392.51s	46.40s	347.94s	35.45s	323.98
16000	59.33s	1341.04s	64.01s	1384.48s	70.76s	1405.00s
32000	131.93s	5929.79s	123.78s	5827.33s	136.22s	5658.81s
64000	245.64s	21584.35s	253.86s	22881.27s	232.30s	21808.43s

Example 4.3. We consider the TFNSE with the following initial conditions:

$$u_1(x,y,0) = \begin{cases} \tanh\big(\rho(y-0.25)\big), & y \le 0.5, \\ \tanh\big(\rho(0.75-y)\big), & y > 0.5, \end{cases}$$
$$u_2(x,y,0) = \varepsilon \sin(2\pi x),$$

where ε is the size of the perturbation and ρ is the shear layer width parameter. In the following experiment, ε is fixed as 0.05. Such initial value problem is used to describe the double shear layer problem in the doubly-periodic unit square [14].

Energy evolution. We set $\nu = 0.1, \rho = 100, T = 50$ and $\alpha = 0.4, 0.6, 0.8$ to compute the numerical solutions. The space discretization is achieved by choosing the Fourier modes as 8×8. The time discretization is achieved by using (4.2). The time interval is split into two parts. The first part is $[0, T_0]$ and the time mesh is calculated as $t_k = T_0(k/N_0)^\delta,\ \delta = 2/\alpha,\ 0 \le k \le N_0$, with $T_0 = 0.01,\ N_0 = 20$. The second part is $[T_0, T]$ and time mesh is calculated by (4.2) with corresponding parameters chosen as $\tau_{\max} = 10^{-1}, \tau_{\min} = 10^{-3}$ and $\eta = 10$. The discrete energy evolution is presented in Fig. 4.6(a). The evolution of the step-sizes with different α is shown in Fig. 4.6(b). We can see, for varying values of α, the energy shows a rapid initial decline. Specifically, a smaller α results in a quicker stabilization of the discrete energy to its steady state. Then, the evolutions of the velocity divergence (4.3) with different α are presented in Fig. 4.7, from which we can see the divergence fluctuations are kept at the machine precision level in the long time simulation.

Furthermore, Fig. 4.8 illustrates the so-called vorticity contours for a thick layer problem with $\nu = 0.0001, \rho = 30$, while Fig. 4.9 shows the contours for a thin layer problem with

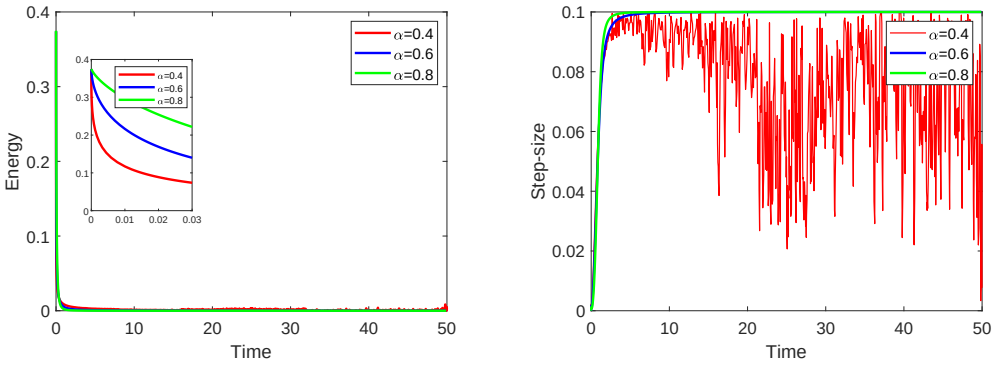

(a) Evolution of discrete energy (b) Evolution of the temporal stepsize

Fig. 4.6. Evolution of discrete energy (a) and temporal stepsizes (b) with $\alpha = 0.4, 0.6, 0.8$ for Example 4.3.

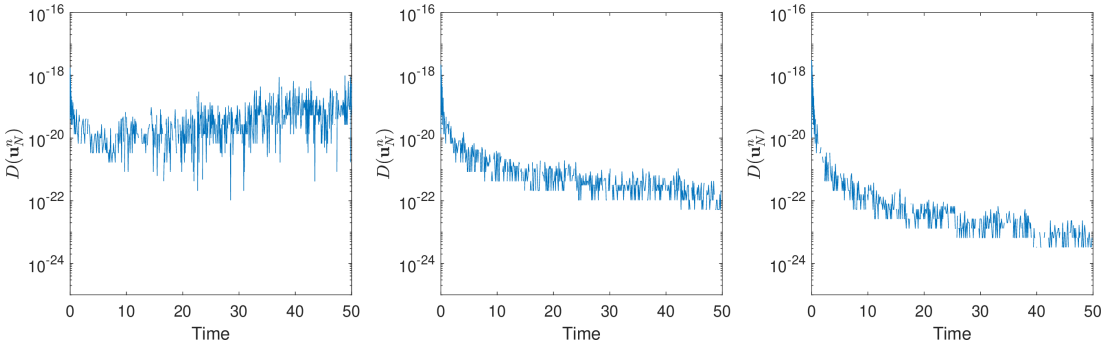

Fig. 4.7. Evolution of velocity divergence with different α: 0.4 (left), 0.6 (middle), 0.8 (right) for Example 4.3.

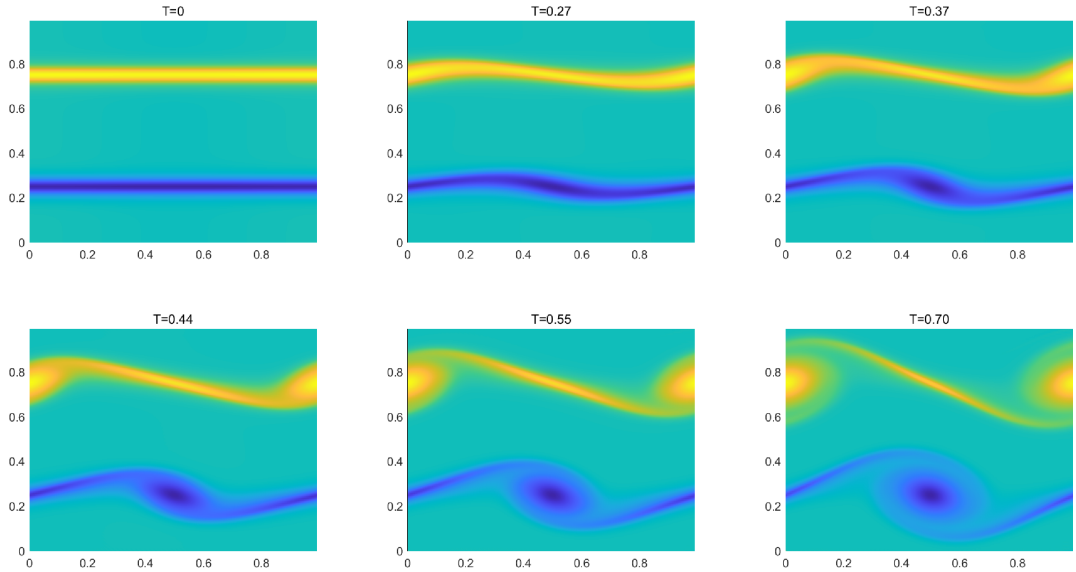

Fig. 4.8. Vorcity contour at $t = 0, 0.27, 0.37, 0.44, 0.55$ 0.70 with $\nu = 0.0001$, $\rho = 30$, and $\alpha = 0.8$ for Example 4.3.

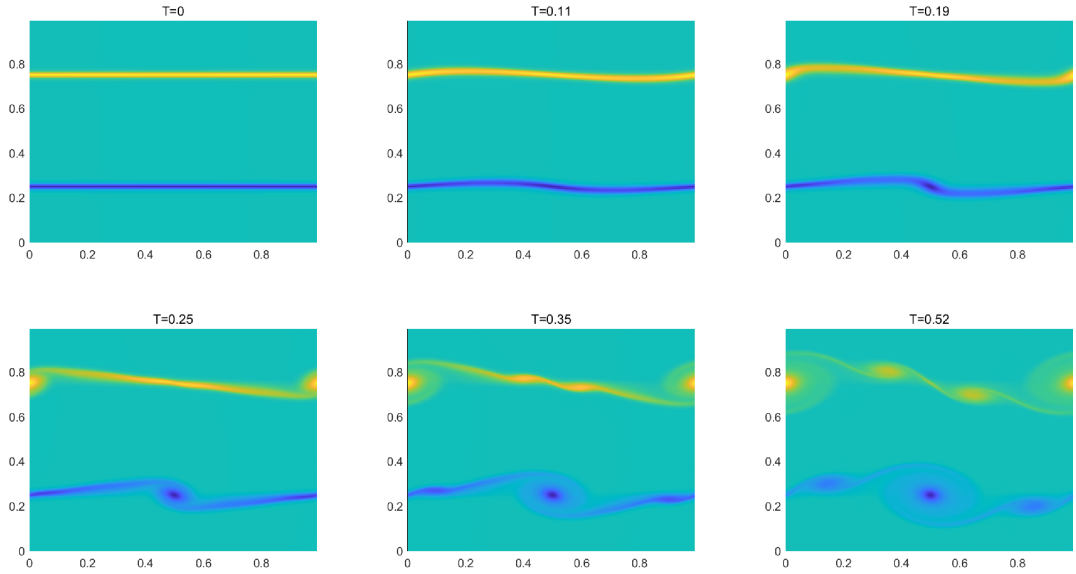

Fig. 4.9. Vorcity contour at $t = 0, 0.11, 0.19, 0.25, 0.30, 0.52$ with $\nu = 0.00005$, $\rho = 100$, and $\alpha = 0.8$ for Example 4.3.

$\nu = 0.00005, \rho = 100$. The space discretization is achieved by choosing the Fourier modes with 128×128. The time discretization is achieved by using (4.2) with $\eta = 10, \tau_{\min} = 10^{-3}, \tau_{\max} = 10^{-1}$.

The figures show the evolution of the vorcity contour in the flow. As the vortex emerges from both ends, it forms the starting primary rings. Later, the vortex splits and wraps around these strong primary rings, resulting in the evolution of a vortex-ring dipole.

Example 4.4. We now consider the problem with the following initial condition:

$$\begin{aligned} u_1(x, y, z, 0) &= \sin(x)\cos(y)\cos(z), \\ u_2(x, y, z, 0) &= -\cos(x)\sin(y)\cos(z), \\ u_3(x, y, z, 0) &= 0. \end{aligned}$$

The domain is chosen as $\Omega := (-\pi, \pi)^3$. The velocity is assumed to satisfy the periodic boundary condition. Such an initial value problem is used to simulate a more general flow [25], the Taylor-Green vortex flow.

Energy evolution. We set $\nu = 0.1,\ T = 50$, and $\alpha = 0.5,\ 0.8$ to compute the numerical solutions. The space discretization is achieved by choosing the Fourier modes as $8 \times 8 \times 8$. The time discretization is achieved by using (4.2). The time interval is divided into two parts. The first part is $[0, 0.01]$ and the time mesh is calculated as $t_k = 0.01(k/N_0)^\delta, \delta = 2/\alpha, 0 \le k \le N_0$ with $N_0 = 20$. The second part is $[0.01, 50]$ and the time step size is calculated by using (4.2) with $\tau_{\min} = 10^{-2}, \tau_{\max} = 10^{-1}$ and $\eta = 10$. The discrete energy evolution is presented in Fig. 4.10(a). The evolution of temporal step-sizes is presented in Fig. 4.10(b). The properties of divergence-free (4.5) are shown in Fig. 4.11. The numerical scheme is shown to satisfy the energy stability discretely.

Moreover, we set the Fourier modes as 32×32×32, and the temporal step sizes by using (4.2). We let $\tau_{\min} = 10^{-2}, \tau_{\max} = 10^{-1}$ and $\eta = 10$. Then, we present the iso-surfaces of $\omega_1^x = -3$ at

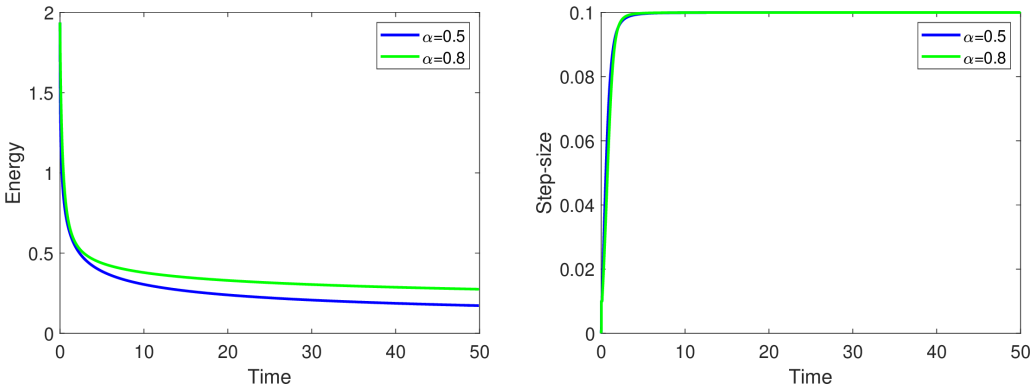

(a) Evolution of discrete energy (b) Evolution of time step-sizes

Fig. 4.10. Evolution of discrete energy (left) and the temporal stepsize (right) with $\alpha = 0.5, 0.8$ for Example 4.4.

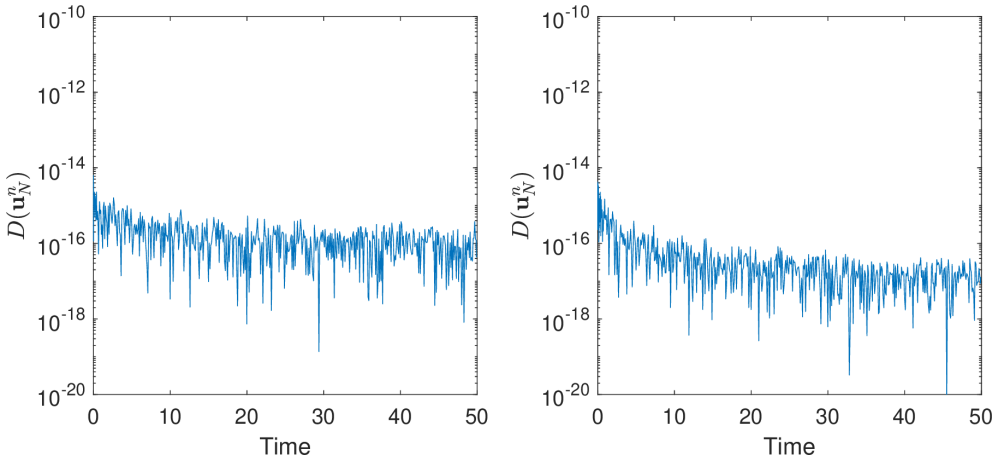

Fig. 4.11. Evolution of velocity divergence with different α: 0.5(left), 0.8(right) for Example 4.4.

different times with $\alpha = 0.8, \nu = 0.005$ in Fig. 4.12. We observe that the flow initially induces eddies of clear structures, which then break up and are finally dissipated by the viscosity.

5. Conclusion

In this paper, we establish a nonuniform $L2-1\sigma$ scheme for solving the TFNSE. The space is discreted by the Fourier spectral methods. The boundedness of the numerical solutions and the discrete energy dissipation are proved. The error estimates of the scheme for the velocity in the sense of L^2-norm is also given. Moreover, we provide an accelerated algorithm to implement the scheme, which can greatly reduce the memory requirement and the computational cost in long-time simulations. Several numerical experiments are presented to confirm the theoretical results, and illustrate the effectiveness and high efficiency of the scheme.

Code and data that allow readers to reproduce the results in this paper are available at `https://github.com/ligroup2000/ruimingao_A-second-order-in-time-and-energy-stable-scheme-for-TFNSE.`

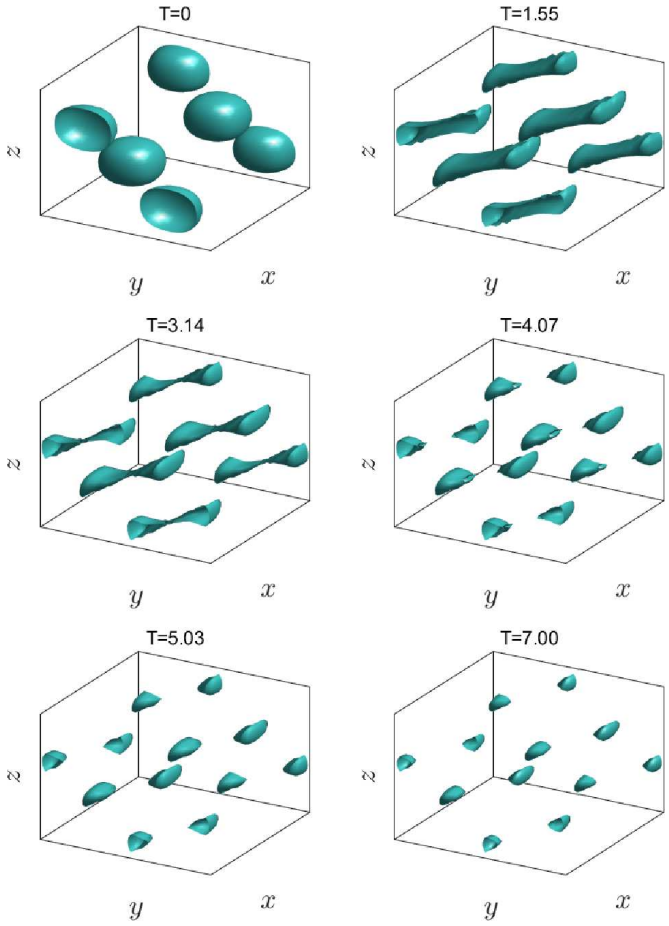

Fig. 4.12. Iso-surface of $\omega_1^x = -3$ at $t = 0, 1.55, 3.14, 4.07, 5.03, 7.00$ with $\alpha = 0.8, \nu = 0.005$ for Example 4.4.

Acknowledgments. The research was supported by the National Natural Science Foundation of China (Grant Nos. 12231003, 12571426) and by the Fundamental Research Funds for the Central Universities of HUST (Grants No. YCJJ20252108). The computation is completed in the HPC Platform of Huazhong University of Science and Technology.

References

[1] S.C. Brenner and L.R. Scott, *The Mathematical Theory of Finite Element Methods*, in: *Texts in Applied Mathematics*, Vol. 15, Springer, 2008.

[2] W. Cai, W. Sun, J. Wang, and Z. Yang, Optimal L^2 error estimates of unconditionally stable finite element schemes for the Cahn-Hilliard-Navier-Stokes system, *SIAM J. Numer. Anal.*, **61**:3 (2023), 1218–1245.

[3] P.M. Carvalho-Neto, *Fractional Differential Equations: A Novel Study of Local and Global Solutions in Banach Spaces*, PhD Thesis, Universidade de São Carlos, 2013.

[4] P. Carvalho-Neto and G. Planas, Mild solutions to the time fractional Navier-Stokes equations in R^N, *J. Differential Equations*, **259**:7 (2015), 2948–2980.

[5] J.W. Cholewa and T. Dlotko, Fractional Navier-Stokes equations, *Discrete Contin. Dyn. Syst. Ser. B*, **23**:8 (2018), 2967–2988.
[6] Q. Du, J. Yang, and Z. Zhou, Time-fractional Allen-Cahn equations: Analysis and numerical methods, *J. Sci. Comput.*, **85** (2022), 42.
[7] R.A. El-Nabulsi, Fractional Navier-Stokes equation from fractional velocity arguments and its implications in fluid flows and microfilaments, *Int. J. Nonlinear Sci. Numer. Simul.*, **20**:3-4 (2019), 449–459.
[8] M. El-Shahed, and A. Salem, On the generalized Navier-Stokes equations, *Appl. Math. Comput.*, **156**:1 (2004), 287–293.
[9] M.A. Fontecha-Medina and E.J. Villamizar-Roa, Global existence and asymptotic behavior of solutions for a fractional chemotaxis-Navier-Stokes system, *Dyn. Partial Differ. Equ.*, **19** (2022), 285–309.
[10] R. Gao, D. Li, Y. Li, and Y. Yin, An energy-stable and divergence-free variable-step L1 scheme for time-fractional Navier-Stokes equations, *Phys. D*, **467** (2024), 134264.
[11] S. Grossmann and D. Lohse, Intermittency in the Navier-Stokes dynamics, *Z. Phys. B: Condens. Matter*, **89** (1992), 11–19.
[12] A.S. Hendy, M.A. Zaky, and J.E. Macías-Díaz, On the dissipativity of some Caputo time-fractional subdiffusion models in multiple dimensions: Theoretical and numerical investigations, *J. Comput. Appl. Math.*, **400** (2022), 113748.
[13] D. Hou and J. Xu, Highly efficient and energy dissipative schemes for the time fractional Allen-Cahn equation, *SIAM J. Sci. Comput.*, **43**:5 (2021), A3305–A3327.
[14] F. Huang and J. Shen, Stability and error analysis of a class of high-order IMEX schemes for Navier-Stokes equations with periodic boundary conditions, *SIAM J. Numer. Anal.*, **59**:6 (2021), 2926–2954.
[15] B. Ji, H. Liao, Y. Gong, and L. Zhang, Adaptive linear second-order energy stable schemes for time-fractional Allen-Cahn equation with volume constraint, *Commun. Nonlinear Sci. Numer. Simul.*, **90** (2020), 105366.
[16] S. Jiang, L. Greengard, and S. Wang, Efficient sum-of-exponentials approximations for the heat kernel and their applications, *Adv. Comput. Math.*, **41** (2015), 529–551.
[17] S. Jiang, J. Zhang, Q. Zhang, and Z. Zhang, Fast evaluation of the Caputo fractional derivative and its applications to fractional diffusion equations, *Commun. Comput. Phys.*, **21**:3 (2017), 650–678.
[18] B. Jin, R. Lazarov, and Z. Zhou, Numerical methods for time-fractional evolution equations with nonsmooth data: A concise overview, *Comput. Methods Appl. Mech. Engrg.*, **346** (2019), 332–358.
[19] B. Jin, B. Li, and Z. Zhou, Correction of high-order BDF convolution quadrature for fractional evolution equations, *SIAM J. Sci. Comput.*, **39**:6 (2017), A3129–A3152.
[20] M.L. Kavvas and A. Ercan, Generalizations of incompressible and compressible Navier-Stokes equations to fractional time and multi-fractional space, *Sci. Rep.*, **12** (2022), 19337.
[21] M.L. Kavvas, A. Ercan, and J. Polsinelli, Governing equations of transient soil water flow and soil water flux in multi-dimensional fractional anisotropic media and fractional time, *Hydrol. Earth Syst. Sci.*, **21** (2017), 1547–1557.
[22] N. Kopteva, Error analysis of an L2-type method on graded meshes for a fractional-order parabolic problem, *Math. Comput.*, **90** (2021), 19–40.
[23] H. Kreiss and J. Oliger, Stability of the Fourier method, *SIAM J. Numer. Anal.*, **16** (1979), 421–433.
[24] C. Li and Z. Wang, Numerical methods for the time fractional convection-diffusion-reaction equation, *Numer. Funct. Anal. Optim.*, **42**:10 (2021), 1115–1153.
[25] D. Li, X. Li, and J. Yang, Relaxation exponential Runge-Kutta methods and their applications to semilinear dissipative/conservative systems, *Commun. Comput. Phys.*, **36**:4 (2024), 908–942.
[26] D. Li, H. Liao, W. Sun, J. Wang, and J. Zhang, Analysis of $L1$-Galerkin FEMs for time-fractional nonlinear parabolic problems, *Commun. Comput. Phys.*, **24**:1 (2018), 86–103.

[27] D. Li, M. She, H. Sun, and X. Yan, A novel discrete fractional Grönwall type inequality and its application in pointwise-in-time error estimates, *J. Sci. Comput.*, **91** (2022), 27.
[28] D. Li, C. Wu, and Z. Zhang, Linearized Galerkin FEMs for nonlinear time fractional parabolic problems with non-smooth solutions in time direction, *J. Sci. Comput.*, **80**:1 (2019), 403–419.
[29] J. Li, A fast time stepping method for evaluating fractional integrals, *SIAM J. Sci. Comput.*, **31**:6 (2010), 4696–4714.
[30] H. Liao, D. Li, and J. Zhang, Sharp error estimate of the nonuniform L1 formula for linear reaction-subdiffusion equations, *SIAM J. Numer. Anal.*, **56**:2 (2018), 1112–1133.
[31] H. Liao, W. McLean, and J. Zhang, A discrete Grönwall inequality with application to numerical schemes for subdiffusion problems, *SIAM J. Numer. Anal.*, **57**:1 (2019), 218–237.
[32] H. Liao, W. McLean, and J. Zhang, A second-order scheme with nonuniform time steps for a linear reaction-subdiffusion problem, *Commun. Comput. Phys.*, **30**:2 (2021), 567–601.
[33] H. Liao, T. Tang, and T. Zhou, A second-order and nonuniform time-stepping maximum-principle preserving scheme for time-fractional Allen-Cahn equations, *J. Comput. Phys.*, **414** (2020), 109473.
[34] H. Liao, X. Zhu, and H. Sun, Asymptotically compatible energy and dissipation law of the nonuniform $L2-1\sigma$ scheme for time fractional Allen-Cahn model, *J. Sci. Comput.*, **99** (2024), 46.
[35] W. McLean, Fast summation by interval clustering for an evolution equation with memory, *SIAM J. Sci. Comput.*, **34**:6 (2012), A3039–A3056.
[36] H. Qin, D. Li, and Z. Zhang, A novel scheme to capture the initial dramatic evolutions of nonlinear subdiffusion equations, *J. Sci. Comput.*, **89** (2021), 65.
[37] J. Ren, H. Liao, J. Zhang, and Z. Zhang, Sharp H^1-norm error estimates of two time-stepping schemes for reaction-subdiffusion problems, *Commun. Comput. Phys.*, **389** (2021), 113352.
[38] M. She, D. Li, and H. Sun, A transformed L1 method for solving the multi-term time-fractional diffusion problem, *Math. Comput. Simulation*, **193** (2022), 584–606.
[39] J. Shen, J. Ren, and S. Chen, A second-order energy stable and nonuniform time-stepping scheme for time fractional Burgers' equation, *Comput. Math. Appl.*, **123** (2022), 227–240.
[40] M. Stynes, E. O'Riordan, and J.L. Gracia, Error analysis of a finite difference method on graded meshes for a time-fractional diffusion equation, *SIAM J. Numer. Anal.*, **55** (2017), 1057–1079.
[41] T. Tang, H. Yu, and T. Zhou, On energy dissipation theory and numerical stability for time-fractional phase-field equations, *SIAM J. Sci. Comput.*, **41**:6 (2019), A3757–A3778.
[42] M.Y. Xu and W.C. Tan, Intermediate processes and critical phenomena: Theory, method and progress of fractional operators and their applications to modern mechanics, *Sci. China Phys., Mech. Astron.*, **49**:3 (2006), 257–272.
[43] Z. Xue and X. Zhao, Compatible energy dissipation of the variable-step L1 scheme for the space-time fractional Cahn-Hilliard equation, *SIAM J. Sci. Comput.*, **5**:45 (2023), A2539–A2560.
[44] Z. Yong and P. Li, On the time-fractional Navier–Stokes equations, *Comput. Math. Appl.*, **73** (2017), 874–891.
[45] F. Zeng, Z. Zhang, and G.E. Karniadakis, Second-order numerical methods for multi-term fractional differential equations: Smooth and non-smooth solutions, *Comput. Methods Appl. Mech. Engrg.*, **327** (2017), 478–502.
[46] G. Zhang, C. Huang, A.A. Alikhanov, and B. Yin, A high-order discrete energy decay and maximum-principle preserving scheme for time fractional Allen-Cahn equation, *J. Sci. Comput.*, **96** (2023), 39.
[47] X. Zhao, R. Yang, R. Qi, and H. Sun, Energy stability and convergence of variable-step L1 scheme for the time fractional Swift-Hohenberg model, *Fract. Calc. Appl. Anal.*, **27** (2024), 82–101.
[48] Z. Zheng, X. Ni, and J. He, Lagrange multiplier structure-preserving algorithm for time-fractional Allen-Cahn equation, *Comput. Math. Appl.*, **164** (2024), 67–78.
[49] Y. Zhou and L. Peng, On the time-fractional Navier-Stokes equations, *Comput. Math. Appl.*, **73**:6 (2017), 874–891.